

Prototype Filters and Filtered Waveforms for Radio Air-Interfaces: A Review

M.Y BENDIMERAD*, S.SENHADJI and F.T.BENDIMERAD

*Department of Electrical Engineering, University of Bechar
LTT Laboratory, University of Tlemcen

Abstract—The perspective for the next generation of wireless communications prognosticates that the communication should take place with high heterogeneity in terms of services and specifications. The emergence of new communication networks, especially between devices like internet of things (IoT) networks, machine type communications (MTC) and unmanned aerial vehicles (UAV), makes the redesign of the radio air-interfaces even higher significant. High data rate, efficient use of the spectrum, low latency, flexibility, scalable ability, energy efficiency and reduced complexity are in the vanguard of the challenging needs. This highlights the necessity to overrides classical waveforms and propose new air interface that best fits these requirements. Several attempts were conducted to propose the most suitable prototype filters and their associated waveforms that support the future applications with these crucial prerequisites. In the present paper, we analyze the most important marked prototype filters reported in literature, and their corresponding waveforms proposed as prominent candidates for wireless air interface. We will show that the filter properties impact the waveform performances and that a close filter-waveform interrelationship is there. The principal contribution is to give a deep insight on the structure of these filters and waveforms and to come up with a fair comparison regarding different criteria and distinct figures of merit.

Index Terms—Prototype filters, Filtered waveforms, B5G-NR, B5G modulations.

I. INTRODUCTION

Since the first generation, mobile wireless communication systems have known a steady evolution. Four generations of the cellular networks have been established and standardized up to now, initiated by the first analogue generation where only voice communication was ensured (AMPS), they evolved then toward digital generations: Global System for Mobile Communications (GSM), General Packet Radio Service (GPRS), Enhanced Data Rates for GSM Evolution (EDGE), Universal Mobile Telecommunications System (UMTS), Long-Term Evolution (LTE) and LTE-A, all characterized by high capacity, diversity and quality of services. The digital processing of the data has contributed significantly to this evolution in the sense that it makes information more flexible to be handled. The emergence of new applications, like internet of things (IoT), e-healthcare, device to device (D2D), machine to machine (M2M), unmanned aerial vehicles (UAV) and machine type communications (MTC) are creating a significant challenge on cellular networks. These are expected to support of tens of thousands of devices connected simultaneously [1][2]. For instance, the ultra-reliable low latency communications (URLLC) requires high reliability, a data rate about 1Gpbs,

an ultra-accurate device positioning and latency less than 1 ms. The enhanced mobile broadband (eMBB) scenario should maintain very large bandwidth allocation in the range of 6 – 90 GHz with a data rate up to 10 Gbps. Also, D2D applications are expected to enable a direct communication between devices in proximity, they require therefore a high energy efficiency and a low latency. Hence, the primary concern is to satisfy the exponential rise in user and traffic capacity. On the other hand, it is essential to decrease the latency and the control signaling to ensure a great autonomy of the device [3]. To this concern, new research areas are explored, like Massive Multiple-Input Multiple-Output (mMIMO), small cells, Coordinated Multi-Point (CoMP), millimeter wave (mmwave) communications and beam-forming techniques. These approaches are essential for 5G and beyond 5G (B5G) wireless networks. B5G technology is expected to be a leading infrastructure for communication industry with a focus on intelligence involvement. Artificial intelligence (AI) and machine learning (ML) are increasingly incorporated in solving problems dealing with the physical layer interface. More specifically, ML and AI were recently used in channel learning and path-loss prediction, as well as in latency and energy consumption reduction [4].

To support all these technologies, different physical-layer air interfaces have been investigated and proposed in literature. The air interface specifies procedures of adapting information to a wireless communication medium. The symbols transmitted via an air-interface belong to a constellation, i.e., Phase-shift keying (PSK) or Quadrature amplitude modulation (QAM). In this case, shaping pulses must maintain maximum spectral efficiency. A pulse shape or prototype filter describes how energy is distributed (in time, frequency) or any other dimension. It is a key factor to show the energy dispersion of the signal and to identify the multi-carrier structure, i.e., orthogonal, non-orthogonal or bi-orthogonal. If the prototype filter involved at the transmitted side and the received side, do not show any correlation in all time-frequency (TF) lattice points, the scheme is either bi-orthogonal or orthogonal. When orthogonal structures maximize the signal to noise (SNR), bi-orthogonal structures may reach better performance for dispersive channels. In literature, different criteria are adopted in the conception of prototype filters: energy concentration ([5],[6]), transition band decay [7], [8] and hardware implementation [9], etc. The rectangular pulse, although perfectly localized in time, shows a bad localization in frequency. This produces interference between carriers in frequency selective channels

[5]. To overcome this drawback, it is possible to lengthen the time symbol, as for sub-critical density or over-sampled modulations [10]. In this case, a decrease in spectral efficiency is noted. Using short-time pulse shape, like rectangular function, reduces the computational complexity and communications latency. Nevertheless, these finite length filters cause high spectral leakage. To cope with, prolate spheroidal wave functions (PSWFs) were proposed. They are time-limited filters with small side-lobes [11], [12]. The Hermite–Gaussian functions are special cases of PSWFs which provide optimum TF concentration. However, these functions don't satisfy the Nyquist criterion. A linear deformation of the Gaussian pulse by Hermit functions leads to the design of Hermite filter [8]. By this way, the Nyquist criterion is fulfilled. Half Square Root Raised Cosine Function (SRRC) is devoted to satisfy Nyquist criterion after matching filtering. It takes advantage from the excellent compromise of TF behavior [13], [14]. The Isotropic Orthogonal Transform Algorithm (IOTA) keeps the good concentration property of Gaussian filter, and adds orthogonality to prevent adjacent interference [15]. It is shown in [16] that an analytical expression can be derived for the IOTA algorithm, which makes the function more tractable. This pulse is called extended Gaussian function (EGF). It achieves exactly the same responses in time and frequency domain [17]. Mirabbasi-Martin functions were proposed to ensure a good transition band decaying property. They exhibit the distinctive that their derivative functions are continuous [18]. The European Physical layer for Dynamic Access (PHY-DYAS) project investigates on the possibility of adapting Mirabbasi-Martin functions to multi-carrier filter bank scheme.

Multi-carrier modulations have the advantage to be robust to multi-path channels. Orthogonal frequency division multiplexing (OFDM) consists in the division of the overall transmission bandwidth into several narrower parallel sub-channels, each of them transmitting a lower-rate signal, which can be decoded efficiently through a simple one-tap equalizer [19] [20]. Although OFDM technique has been adopted as the air interface in several wireless communication standards, it exhibits some intrinsic drawbacks. These make OFDM unsuitable to be adopted in specific contexts as double dispersive channel environments [21]. The spectral efficiency (SE) loss caused by cyclic prefix insertion and the synchronization required for orthogonality are the major shortcomings for the orthogonal OFDM signaling technique. In these cases, the low complexity of OFDM technique would wear off as synchronization algorithms are inducted with high-level of calculation [22]. OFDM also suffers from other critical problems such as the great peak to average power ratio (PAPR) when the number of sub-carriers is important and the high side lobes due to the rectangular transmitting filter. Some solutions have been proposed to overcome the aforementioned OFDM's drawbacks, like relaxing the tight synchronization by proposing algorithms for multi-user interference cancellation [23] [24], or for reducing out-of-band leakage [25]. However, all these methods are generally very complex to implement and they increase the receiver calculations. In these circumstances, Filtered Bank Multi Carrier (FBMC) modulation was proposed to replace OFDM [14]. While relying on dividing the spectrum

into multiple sub-bands, too, FBMC applies a filtering function to each of the sub-carriers. Therefore, the side-lobes are much weaker and thus the inter-carrier interference (ICI) issue is by far less crucial than with OFDM [26]. Therefore, a system applying FBMC is much more suited to a potential 5G or beyond 5G (B5G) system in that respect [26] [27]. Although FBMC theory reveals a set of valorous features, most of them are practically neglected, due their no feasibility and difficult implementation. Recent tendencies try to design waveforms or their equivalent prototype filters that reunite the theoretical advantages and a simple practical implementation [28] [29] [30] [31]. New waveforms using well-shaped filters have achieved great attention recently. These are : generalized frequency division multiplexing (GFDM) [32], universal filtered multi-carrier (UFMC) [33][11] filtered orthogonal frequency division multiplexing (F-OFDM) [34] and windowed orthogonal frequency division multiplexing (W-OFDM) [35].

In the subsequent paragraphs, we will try to analyze and compare the performances of all these prototype filters and all these multi-carrier modulation schemes. The major contributions of the present paper are listed as follows:

- A review of the state of the art regarding the mathematical formulations and the design methods of filter functions.
- An investigation on the selection criteria between prototype filters.
- A review of the most prominent filtered multi-carrier modulation (MCM) schemes meeting the aforementioned requirements.
- An exhaustive comparison between MCM schemes based on several key performance indicators and within different scenarios.

The paper is outline as follows: section (2) reviews the state-of-the art of prototype filters. Section (3) assesses the filters performance and the selection criteria. Section (4) approaches the different filtered waveforms from a structural point of view. In section (5), we discuss the assessment of these waveforms in different contexts and under various conditions. Meaningful outcomes on the filter-waveform dependency in respect of this review are marked in section (6). Section (7) concludes this survey.

a) Notations: For best clearness and readability, we define in this part the notations used in the subsequent sections. These have for meaning that specified in the following table; except if in the text it is mentioned that the notation has another connotation.

II. PROTOTYPE FILTERS

In parallel transmitting data systems, each channel occupies a relatively narrow frequency band. In this case, it is tempting to avoid spectral overlap of the channels to drop inter-channel interference. However, higher signaling rates can be achieved if spectral overlap is permitted [36]. In multi-carrier systems, modulated signal can be represented as a linear combination of a Gabor family (P, T_0, F_0) [37], where T_0 is the symbol duration of the modulated signal, F_0 inter carrier spacing and

Parameters	Definition
A_p	Ambiguity function
E	Energy
e	Exponential function
f	Frequency
F_0	Frequency duration
h	Impulse response
h_n	Hermite function
H	Transfer function
i	Complex variable
i, k, l, m	Natural variables
L_F	Filter length
n	Discrete time
N_B	Number of blocks
r	Roll-off factor
t	Continuous time
T_c	Coherence time
T_0	Signaling duration
T_{CP}	Cyclic prefix duration
T_{ZP}	Zero padding duration
T_{GS}	Guard symbol duration
u	Real variable
τ	Time delay
ν	Doppler frequency
τ_0	Carriers orthogonality duration
ν_0	Inter-carrier distance
ω	Angular frequency
δ	Standard deviation

P the prototype filter pulse. Balian-low theorem states that no modulation scheme can satisfy complex orthogonality, Nyquist rate criterion and have a good time-frequency localization (TFL) at the same time. A straightforward proof example of the theorem is Cyclic-Prefix OFDM (CP-OFDM) scheme. The Heisenberg-Gabor uncertainty is given by:

$$\delta_t \delta_f \geq \frac{1}{4\pi} \quad (1)$$

Where δ_t and δ_f are respectively the time and frequency standard deviation. It means that the product of the localization uncertainties in frequency and time must exceed a fixed constant. It is significant to note that for Gaussian pulse, the equality holds due to the symmetry property of Gaussian function. Although Gaussian pulse is optimal in the sense that it presents equal spreading in both time and frequency domain, unfortunately, its pulse does not satisfy the Nyquist inter symbol interference (ISI) and inter carrier interference (ICI) cancellation property[13].

A. Rectangular Filter

The rectangular function is the prototype filter used for the conventional OFDM transmission scheme. This filter distributes uniformly the energy carried by a symbol through the time domain. At the transmitter its duration can be enlarged so it can effectively combat inter-symbol and inter-carrier interference in time invariant multi-path channels. Its analytical expression is [38] :

$$\text{rect}(t) = \begin{cases} 1 & |t| < \frac{1}{2} \\ 0 & \text{elsewhere} \end{cases} \quad (2)$$

By multiplying with a suitable displaced rectangle function, it is possible to select any segment of any function. The characteristics of the rectangular filter play a significant role

in determining the resulting frequency response of the OFDM system. Specifically, the convolution with the rectangular function has the effect of smoothing the signal [39]. The Fourier transform of rectangular filter is :

$$\text{RECT}(\omega) = \frac{1}{\sqrt{2\pi}} \frac{\sin(\frac{\omega}{2})}{\frac{\omega}{2}} \quad (3)$$

With: $\omega = 2\pi f$

The implementation of a long duration rectangular filter can be considerable even after truncation. Rectangular filter accounts for a good benchmark for comparison.

B. Raised Cosine Filter

In data communication systems, the transmitted signal must be restricted to a certain bandwidth. This can be due to either system design constraints or regulations [40]. Thus, the choice of a filter must serve to reduce the effective bandwidth while maintaining cancellation of time interference. Raised cosine filter, takes on the shape of a sinus cardinal pulse. This filter has the property of vestigial symmetry. This means that its spectrum exhibits odd symmetry. The transfer function of the raised cosine filter is[41]:

$$H_1(\omega) = \begin{cases} A & |\omega| < \omega_1 \\ \frac{A}{2}(1 + \cos(\pi \frac{|\omega| - \omega_1}{r\omega_c})) & \omega_1 \leq |\omega| \leq \omega_2 \\ 0 & |\omega| > \omega_2 \end{cases} \quad (4)$$

With: $\omega_1 = \frac{1-r}{2}\omega_c$, $\omega_2 = \frac{1+r}{2}\omega_c$, $A = \frac{2\pi}{\omega_c} = T_c$, ω_c the central pulsation and r the roll-off factor.

The energy is calculated by integrating the module of $H_1(\omega)$ over \mathbb{R} .

$$E_{H_1} = \int_{-\infty}^{+\infty} |H_1(\omega)|^2 d\omega = \frac{\pi^2}{\omega_c} (4 - r) \quad (5)$$

It is common to implement raised cosine response by two identical filters, one implemented at emitter side and another at receiver side. In such cases, the response becomes a square-root raised cosine. The transfer function of the root-raised cosine filter is [41]:

$$H_2(\omega) = \begin{cases} B & |\omega| < \omega_1 \\ \frac{B}{\sqrt{2}} \sqrt{1 + \cos(\pi \frac{|\omega| - \omega_1}{r\omega_c})} & \omega_1 \leq |\omega| \leq \omega_2 \\ 0 & |\omega| > \omega_2 \end{cases} \quad (6)$$

With : $B = \sqrt{T_c}$

The total energy is:

$$E_{H_2} = \int_{-\infty}^{+\infty} |H_2(\omega)|^2 d\omega = 2\pi \quad (7)$$

The impulse response of the root raised cosine filter is assumed as a real and an even function. Applying inverse Fourier transform, one can write [41]:

$$h_2(t) = \int_{-\infty}^{+\infty} H_2(\omega) e^{i\omega t} d\omega \quad (8)$$

$$h_2(t) = C \frac{\sin\left((1-r)\pi\frac{t}{T_c}\right) + 4r\frac{t}{T_c} \cos\left((1+r)\pi\frac{t}{T_c}\right)}{\pi\frac{t}{T_c} \left(1 - \left(4r\frac{t}{T_c}\right)^2\right)} \quad (9)$$

$$\text{With : } C = \frac{B}{T_c} = \frac{1}{\sqrt{T_c}}$$

The square-root raised cosine frequency response is depicted in Fig.1.

The SRRC filter characteristic can be adjusted via the roll-off parameter r that belongs to the interval $[0, 1]$. Depending on the value of r , the square-root raised cosine power spectral density (PSD) can have large or narrow main lobe and great or small side-lobes. Note that as the r value increases from zero to one, the passband of the filter increases while the amplitude of the time domain ripples decreases. Moreover, to get a realizable SRRC filter, the roll-off factor must be different from zero.

C. Hermite Filter

Works on Hermite functions, aim to find a base function with dispersion product even closer to the uncertainty limit of equation (1) while satisfying the necessary orthogonality properties. Thus, the chosen base functions must be invariant when applying the Fourier transform as with Gaussian pulses. The used Hermite functions are [42] :

$$h_n(t) = e^{-\frac{t^2}{2}} \frac{d^n}{dt^n} e^{-t^2} \quad (10)$$

Which verify:

$$\lambda \cdot h_n(t) = \int_{-\infty}^{+\infty} h_n(f) e^{ift} df \quad (11)$$

$$\text{Where: } \lambda = \lambda_n = j^n \sqrt{2\pi}$$

If we normalized by $D_n(t) = h_n(\sqrt{2\pi}t)$ we get as in [42]:

$$D_n(t) = \int_{-\infty}^{+\infty} D_n(f) e^{i2\pi ft} df \quad (12)$$

It is also demonstrated in [42] that the pulse shape $h(t)$ formed by linear combination of $D_n(t)$, when n is multiple of 4, also satisfies this identity:

$$h(t) = \sum_{k=0}^{Q-1} H_{4k} D_{4k}(t) \quad (13)$$

The H_{4k} parameters are chosen so that the orthogonality condition is satisfied. Otherwise, these parameters must lead to a null ambiguity function $A(\tau, \nu)$ at points $\tau = nT_0$ and $\nu = kF_0$. In Fig.1 the H_{4k} coefficients are calculated according to [42] for $Q = 4$.

D. Gaussian Function

Gaussian function constitutes an isotropic prototype function. This means transforming this function by Fourier operation yields no change in the shape. For Gaussian function, the analytical expression is given by [43]:

$$g_\alpha(t) = (2\alpha)^{(1/4)} e^{-\pi\alpha t^2}, \alpha > 0 \quad (14)$$

By getting the Fourier transform, it yields :

$$\begin{aligned} G_\alpha(f) &= (2\alpha)^{(1/4)} \int_{-\infty}^{+\infty} e^{-\pi\alpha t^2} e^{-i2\pi ft} dt \\ &= (2\alpha)^{(1/4)} \sqrt{\frac{\pi}{\pi\alpha}} e^{(-i\pi f)^2 / (\pi\alpha)} \end{aligned} \quad (15)$$

$$= (2/\alpha)^{(1/4)} e^{-i\pi(f)^2/\alpha} = g_{1/\alpha}(f) \quad (16)$$

It is straightforward from the above equation that the Fourier transform of a Gaussian function yields a function with the same shape except for an axis scaling factor. It seems to be an attractive candidate for a pulse shaping prototype function, but it is in no way orthogonal:

$$g_\alpha(t) > 0 \quad (17)$$

E. IOTA Algorithm

The basic functions forming the transmitted signal are got by translation in time and frequency of a prototype function:

$$x_{m,n}(t) = i^{m+n} e^{i2\pi m F_0 t} x(t - nT_0) \quad (18)$$

Here n and m express the time and frequency translation respectively. Commonly $T_0 = F_0 = 1/\sqrt{2}$.

In the case of OFDM, this set of functions is orthonormal and forms a Hilbertian basis. Hilbertian basis provides a powerful tool to design multi-tone systems. A Hilbertian space of square-integrable functions is defined with either standard inner product or real inner product. In[15] for real inner product case, an example of Hilbertian basis of square-integrable functions is obtained with a prototype function defined by its Fourier transform:

$$X(f) = \begin{cases} \frac{A}{\sqrt{F_0}} \cos\left(\frac{\pi f}{2F_0}\right) & |f| < F_0 \\ 0 & elsewhere \end{cases} \quad (19)$$

Consider an orthogonalization factor, denoted O , which aims to orthogonalise a given function over frequency axis. The same function can be orthogonalized over the time axis using the operator defined by $F^{-1}OF$ (F being the Fourier transform). When applied to the function, the O operator cancels the ambiguity function over the frequency axis. Furthermore, we can see the same effect on the ambiguity function over time axis by applying the $F^{-1}OF$ operator. Let's consider the following functions:

$$g_\alpha(t) = \sqrt[4]{2\alpha} \cdot e^{-\pi\alpha t^2} \quad (20)$$

$$G_\alpha = F^{-1}OFg_\alpha(t) \quad (21)$$

It can be demonstrated that:

$$A_{G_\alpha}(n\sqrt{2}, m\sqrt{2}) = 0 \quad (m, n) \neq (0, 0) \quad (22)$$

Where A_{G_α} is the ambiguity function described in equation (38).

Here we have a set of functions that can be taken as the prototype function of a Hilbertian basis depending on the chosen term α . Moreover, this parameter affects the power distribution of the pulse in the time/frequency space[37]. It is important to note that the O operator is defined to satisfy (23). The first orthogonalization step introduces nulls in the ambiguity function in frequency domain while the second orthogonalization step introduces nulls in delay domain [21].

$$y(u) = \frac{2^{\frac{1}{4}}x(u)}{\sqrt{\sum_k \|x(u - \frac{k}{\sqrt{2}})\|^2}} \quad (23)$$

F. Extended Gaussian Function

It is shown in [17] that an analytical expression can be derived for the isotropic orthogonal transform algorithm (IOTA) algorithm given by equation (21). This makes the function $G_\alpha(t)$ in this equation more tractable:

$$G_{\alpha, \tau_0, \nu_0}(t) = \frac{1}{2} \sum_{k=0}^{\infty} d_{k, \alpha, \nu_0} \left[g_\alpha \left(t + \left(\frac{k}{\nu_0} \right) \right) + g_\alpha \left(t - \left(\frac{k}{\nu_0} \right) \right) \right] \\ \times \sum_{l=0}^{\infty} d_{l, \tau_0, 1/\alpha} \cos \left(2\pi l \frac{t}{\tau_0} \right) \quad (24)$$

With d_{k, α, ν_0} a set of real coefficients and $0.264 < \alpha < 1/0.264$.

The practical use of the above equation needs the knowledge of the real coefficients d_{k, α, ν_0} . These are expressed by the following infinite series:

$$d_{k, \alpha, \nu_0} = \sum_{l=0}^{\infty} a_{k, l} e^{-(l\pi/2\nu_0^2)\alpha} \quad (25)$$

We note that we have to compute an infinite set of coefficients $a_{k, l}$. However, it is still possible to truncate the above

expression to a finite set with enough accuracy, due to the fast decreasing of the function G_α [44]. A set of $a_{k, l}$ coefficient is reported in [17] which can be used in calculating the seven first $d_{k, \alpha}$ parameters.

G. Martin Filter

Martin proposes in [7] a linear phase filter based on Lerner filters. The idea is such that a linear combination is performed on a number of Inverse Fourier Transformation/ Fourier Transformation (IFT/FT) adjacent filter channels where the sum of weighting coefficients is fixed to be zero with an alternation in coefficient's sign:

$$T_i(\omega) = \sum_i k_i \text{IFT}_i = \dots + k_{i-2} \text{IFT}_{i-2} + k_{i-1} \text{IFT}_{i-1} \\ + k_i \text{IFT}_i + k_{i+1} \text{IFT}_{i+1} + k_{i+2} \text{IFT}_{i+2} + \dots \quad (26)$$

With:

$$\sum_i k_i = 0 \quad (27)$$

This constraint results in an excellent stop-band performance. The choice of coefficients is paramount for determining the adaptation to a given application scheme. If some choices result for example, in an aliasing for multi-tone communications, others can be acceptable. In [7] filter coefficients are determined for the case where M the number of filter banks, satisfies:

$$M = \begin{cases} n/3 \\ n/4 \\ n/6 \\ n/8 \end{cases} \quad (28)$$

Here, n is the order of IFT. In the case $M = n/3$, five adjacent filters are used, the order of the resulting prototype filter is $n - 1$ and the number of weighting coefficients is $(2n/M) - 1$ [7]:

$$T_{i/3}(\omega) = k_2 \text{IFT}_{i-2} + k_1 \text{IFT}_{i-1} + k_0 \text{IFT}_i \\ + k_1 \text{IFT}_{i+1} + k_2 \text{IFT}_{i+2} \quad (29)$$

Where:

$$\text{IFT}_i(\omega) = \frac{1}{n} \sum_{k=0}^n e^{-j2\pi ik/n} e^{-j\omega kT} \quad (30)$$

Under the constraint that:

$$k_2 + k_1 + k_0 + k_1 + k_2 = 0 \quad (31)$$

Generally, other considerations are taken into account to find filter coefficients, as the unity gain for the sum of transmitting and receiving filters at the IFT center frequencies:

$$\sum_{i=0}^K T_i(\omega) R_i(\omega) = 1 \quad (32)$$

TABLE I
ANALYTICAL EXPRESSION OF PROTOTYPE FILTERS.

Filter	Analytical Expression	Parameters
Rectangular	$h(t) = \begin{cases} 1 & t < \frac{1}{2} \\ 0 & \text{elsewhere} \end{cases}$	
SRRC	$h(t) = C \frac{\sin\left((1-r)\pi\frac{t}{T_c}\right) + 4r\frac{t}{T_c} \cos\left((1+r)\pi\frac{t}{T_c}\right)}{\pi\frac{t}{T_c} \left(1 - \left(4r\frac{t}{T_c}\right)^2\right)}$	$C = \frac{B}{T_c} = \frac{1}{\sqrt{T_c}}, r \in [0, 1]$
Hermite	$h_n(t) = e^{-\frac{t^2}{2}} \frac{d^n}{dt^n} e^{-t^2}$	$Q > 0$
Gaussian	$g_\alpha(t) = (2\alpha)^{(1/4)} e^{-\pi\alpha t^2}$	$\alpha > 0$
IOTA	$h_\alpha(t) = F^{-1} O F O g_\alpha(t)$	$y(u) = \frac{2^{\frac{1}{4}} x(u)}{\sqrt{\sum_k \ x(u - \frac{k}{\sqrt{2}})\ ^2}}$
EGF	$G_{\alpha, \tau_0, \nu_0}(t) = \frac{1}{2} \sum_{k=0}^{\infty} d_{k, \tau_0, \nu_0} \left[g_\alpha\left(t + \left(\frac{k}{\nu_0}\right)\right) + g_\alpha\left(t - \left(\frac{k}{\nu_0}\right)\right) \right] \cdot \sum_{l=0}^{\infty} d_{l, \tau_0, 1/\alpha} \cos\left(2\pi l \frac{t}{\tau_0}\right)$	$d_{k, \alpha, \nu_0} = \sum_{l=0}^{\infty} a_{k, l} e^{-(l\pi/2\nu_0^2)\alpha}$
MARTIN	$T_i(\omega) = \dots + k_{i-1} \text{IFT}_{i-1} + k_i \text{IFT}_i + k_{i+1} \text{IFT}_{i+1} + \dots$	$\text{IFT}_i(\omega) = \frac{1}{n} \sum_{k=0}^n e^{-j2\pi i k/n} e^{-j\omega k T}$
PHYDYAS	$h(t) = 1 + 2 \sum_{k=1}^{K-1} H_k \cos\left(2\pi \frac{kt}{Kt}\right)$	$K = 2, 3, 4$

TABLE II
PAPERS DEALING WITH PROTOTYPE FILTERS.

Filters	Rectangular	SRRC	Hermite	Gaussian	IOTA	EGF	MARTIN	PHYDYAS
Equalization	[83], [84] [85], [86]	[99], [100] [101]	[108]	[109], [85]	[110], [111]		[114], [84] [83], [115]	[114], [120]
Synchronization	[90], [92] [91]	[102], [90] [103]	[102]		[102]	[106], [91]	[114], [116] [92], [117]	[116]
Complexity Analysis	[93], [94] [95]	[104], [105]			[50]		[115]	[115] [1], [2]
Channel Estimation	[96], [97]	[106], [107] [96]			[112], [97] [111]	[106], [97] [96]		[121]
Spectral Leakage	[98], [94] [93]	[94], [93] [89]			[113]		[118]	
PAPR	[87], [88] [89]	[88], [87]					[119]	[119]

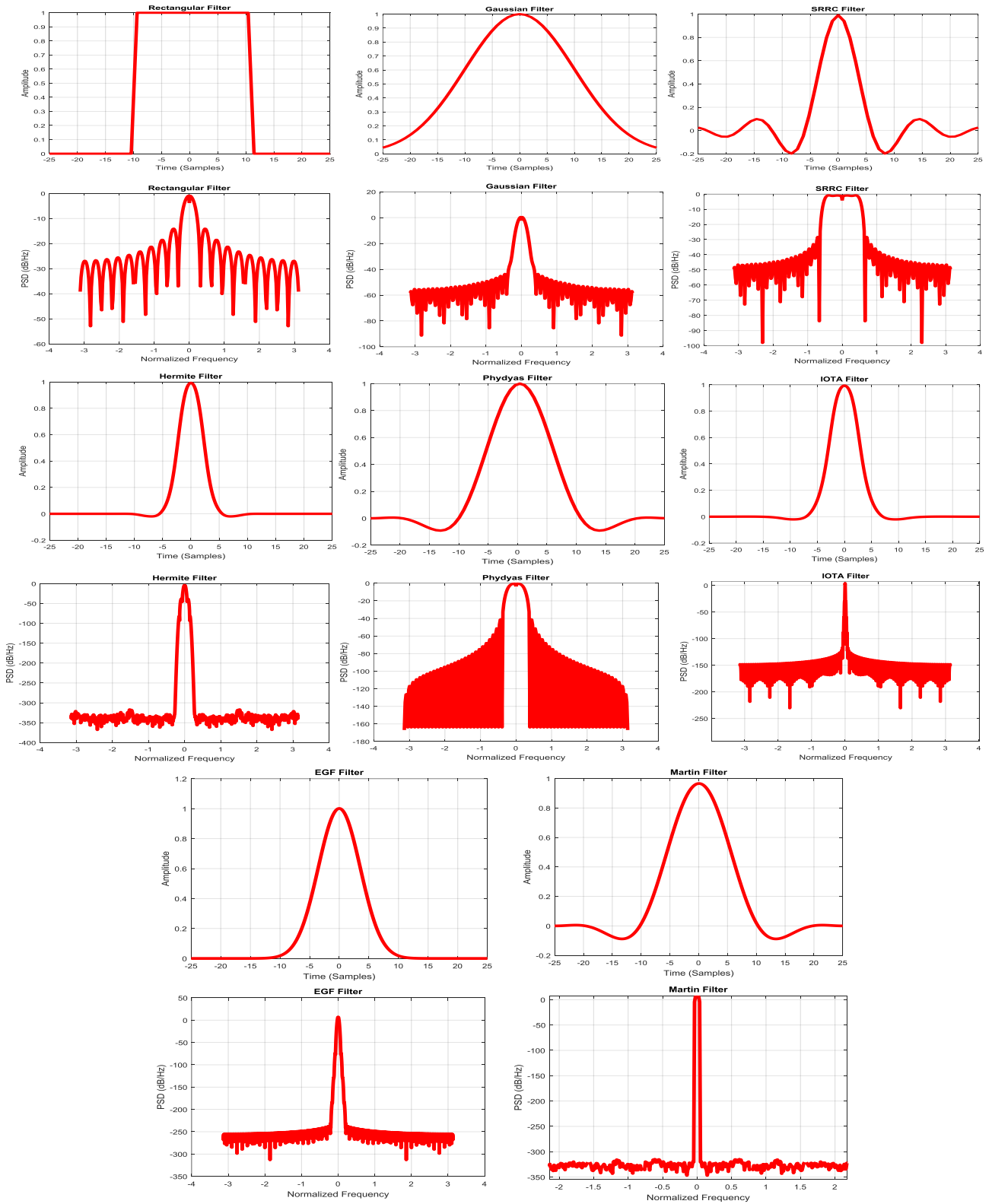


Fig. 1. Time-Frequency representation of Prototype filters

Where: $T_i(\omega)$ are the transmission filters and $R_i(\omega)$ the received ones.

Witch yields:

$$\begin{cases} k_0 = 1 \\ k_1^2 + k_2^2 = 1 \end{cases} \quad (33)$$

H. Phydyas Filter

The design of the PHYDYAS prototype filter is based on a frequency sampling technique. The Nyquist theory imposes that the impulse response of the transmission filter must cross the zero axis at all the integer multiples of the symbol period. In frequency domain, this translates to a symmetry condition about the cutoff frequency. So the design is based on considering the frequency coefficients while imposing symmetry condition [27]. The frequency response of the prototype filter is obtained from the frequency coefficients using an interpolation function:

$$H(f) = \sum_{k=-K+1}^{K-1} H_k \frac{\sin(\pi(f - \frac{k}{MK})MK)}{MK \sin(\pi(f - \frac{k}{MK}))} \quad (34)$$

K represents the overlapping factor and M is the number of sub-channels. In time domain, this yields:

$$h(t) = 1 + 2 \sum_{k=1}^{K-1} H_k \cos\left(2\pi \frac{kt}{Kt}\right) \quad (35)$$

For a discrete time, a close form of the prototype filter for an overlapping factor $K = 4$ is expressed as:

$$h[m] = H[0] + 2 \sum_{k=1}^{K-1} (-1)^k H[k] \cos\left(\frac{2\pi k}{KM}(m+1)\right) \quad (36)$$

Where:

$$\begin{cases} m = 0, 1, \dots, KM - 2 \\ K = 4 \\ H[0] = 1 \\ H[1] = 0.97195983 \\ H[2] = 1/\sqrt{2} \\ H[3] = \sqrt{1 - H[1]} \end{cases} \quad (37)$$

The analytical expressions of prototype filters are shown in [Table.I](#).

III. SELECTION CRITERIA

A. Ambiguity Function Analysis

The orthogonality condition can be investigated through ambiguity function. For a pulse shape $p(t)$, we define his ambiguity function as[45] :

$$A_p(\tau, \nu) = \int_{-\infty}^{+\infty} p\left(t + \frac{T}{2}\right) p^*\left(t - \frac{T}{2}\right) e^{-i2\pi\nu t} dt \quad (38)$$

Where τ is the time delay and ν is the frequency Doppler. In this section, we will examine the set of ambiguity functions calculated for the already studied filters.

The ambiguity function indicates how symbols are spread across the time and frequency axes; a zero crossing of the ambiguity function over time or frequency axis guarantees ISI and ICI free transmission. [Fig.2](#) presents the ambiguity surface for different filter designs. For square root raised cosine filter with a roll-off factor $\alpha = 0.1$ the ambiguity function value attains -10dB (0.1 on color bar) at the points $\nu = \pm 20 \text{ KHz}$ and $\tau = \pm 70 \mu\text{s}$. The ambiguity function reaches a level lower than -50dB (dark blue on the [Fig.2](#)) as $\nu \geq \pm 35 \text{ KHz}$ and $\tau \geq \pm 180 \mu\text{s}$. From the ambiguity surface for the Gaussian filter, we note that the symbol spreading effect over time and frequency equals. This is due the symmetry of the Gaussian function with respect to the Fourier transform. From the [Fig.2](#), one can conclude that in terms of orthogonality, the Gaussian function is not a good choice since it is non-orthogonal and shows a great spreading effect across the time-frequency axes. The IOTA design algorithm presented is based on two orthogonalization parameters; the first introduces nulls in the ambiguity function in frequency domain, while the second introduces nulls in the ambiguity function in the time domain. The space in the figure characterizes by $\nu \geq \pm 10 \text{ KHz}$ and $\tau \geq \pm 250 \mu\text{s}$ are areas where $|A_p| \leq -60\text{dB}$. The Hermite pulse ambiguity function is plotted with parameters $H_{4k} = \{H_0, H_4, H_8, H_{12}\}$ where $H_0 = 1.1850899$. The Hermite pulses suffer from numerical problems, thus its ambiguity function calculation takes a long time in the simulation. It is clear that ambiguity function reaches swiftly lower values as $\nu = \pm 15 \text{ KHz}$; nevertheless, we do not see the same case on a time axis. As for the ambiguity surface of a Phydyas filter with parameters $H_1 = 0.97196$, $H_2 = 0.70710$ and $H_3 = 0.23514$, like previous ambiguity function scheme, it presents high values around $\nu \approx 0 \text{ KHz}$ and $\tau \approx 0 \mu\text{s}$ point, meanwhile it shows some regions near the origin where it decreases rudely as the SRRC, IOTA and Hermite cases. The Martin filter ambiguity function is plotted for the case $K = 6$, time and doppler delay are relatively high for region inside $\tau < \pm 50 \mu\text{s}$ and $\nu < \pm 15 \text{ KHz}$. The ambiguity function reaches low values outside this region. Finally, Regarding EGF filter, ambiguity function exhibits same behavior in time and frequency domain since it is just an extension of Gaussian filter, nevertheless it reaches promptly very low values $|A_p| \leq -60\text{dB}$ as can be deduced.

B. Energy Concentration

In practice, it is always preferable to limit the duration of the pulse shape so that the computational complexity is significantly reduced. However, limiting pulse shape by truncation, for instance, causes high side-lobes in Fourier domain. So How can we obtain a time-limited pulse with least out-of-band leakage or inversely a band-limited pulse with greatest energy concentration within a given interval? The selected prototype filter depending on energy concentration should discuss this trade-off problem. [Fig.3](#), presents a comparison

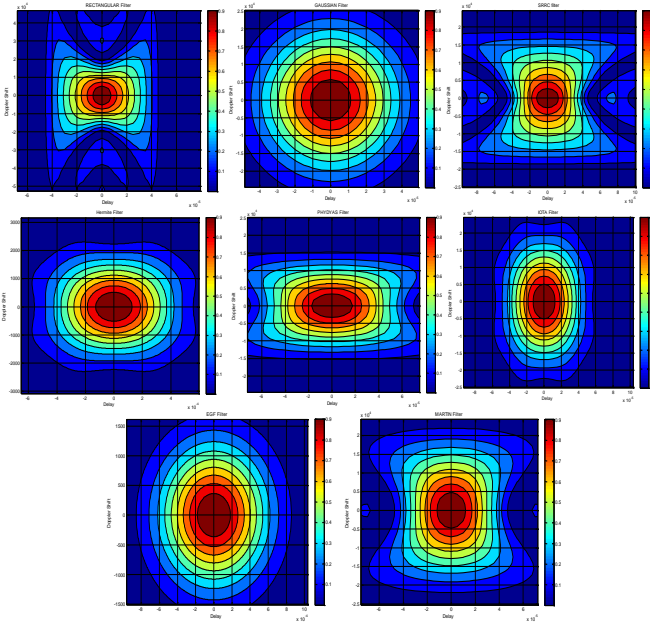


Fig. 2. Ambiguity function.

of all mentioned filters in terms of energy concentration. The rectangular filter energy is shown to be spread out on all frequency domain. This finding is nothing but a direct result of the Balian-Low theorem, which states that no scheme can satisfy simultaneously a good time-frequency localization (TFL). The Gaussian function is another filter with poor energy concentration. This function was subject in several studies to enhance his energy localization and reducing out-of-band leakage. The resulting filters are IOTA and EGF. The bandwidths of these filters at -100dB power level are 5Hz and 12Hz , respectively. The EGF is plotted with α parameter equals $1/2$. It is important to note that an increase in the value of α improves spectral efficiency of the filter. The SRRC filter shows a good energy concentration at the expense of a nearly constant side-lobes, its bandwidth at -100 is 10Hz . Martin and Hermite filters exhibit large main lobe with a bandwidth of 10Hz and 11Hz at power levels -70dB and -80dB , respectively. As for Phydias filter, its main lobe bandwidth is about 60Hz at -70dB .

C. Transition Band Decay

In many applications, it is preferable for a given transmitting model that the side-lobes decay rapidly rather than remaining constant. The motivation behind this is to reduce considerably interference among adjacent users. It is known that the side-lobes falling rate is related to the number of continuous derivatives, this one is nothing but a filter's smoothing measure [46] [47]. Fig.4, shows the decaying property for the different presented prototype filters in the frequency domain. Due to the well localization of the rectangular filter in the time domain, it has no significant decay in the frequency domain and the side-lobes remain constant around -40dB . Gaussian filter shows also a slow decay until 120Hz , then the side-lobes remain nearly constant around -160dB . The Phydias and SRRC

filters evince a similar decay behavior with a difference of about 20dB that increases with frequency, since SRRC side-lobes come to be constant with frequency. For the Martin filter, the coefficient calculation leads to continuous derivatives of the function which ensure a magnificent falling property. The continuous decay of side-lobes is well established in the Fig.4. IOTA, EGF and Hermite filters show the fast decaying property among all filters. The PSD of the three filters reaches a very low thresholds about -160dB only for the first 20Hz band. Depending on the chosen α coefficient, the EGF filter exhibits roughly good results. IOTA is a particular EGF filter derived from a mathematical closed-form expression with $\alpha = 1$. For Hermite filter the slope characteristic of the PSD can be further enhanced by increasing the filter order Q at the expense of an increase in complexity.

IV. FILTERED WAVEFORMS

Considering the needs of upcoming applications in wireless communications, new filtered waveforms have been studied to be adopted in physical communication layer. These ones include several novel prototype filters which provide a good frequency localization and reduce the out-of-band radiation. Some techniques as Filter-Bank Multi-Carrier Offset QAM (FBMC-OQAM) and GFDM try to filter each sub-carrier separately to get a tight time-frequency localization in each sub-carrier, while others like F-OFDM apply the filter to the whole occupied band or to groups of consecutive sub-carriers as UFMC technique to reduce the Out-of-band (OOB) leakage.

A. CP-OFDM

The single-carrier frequency division multiple access (SC-FDMA) and CP-OFDM techniques are used respectively in the up-link and down-link of the actual LTE systems. SC-FDMA

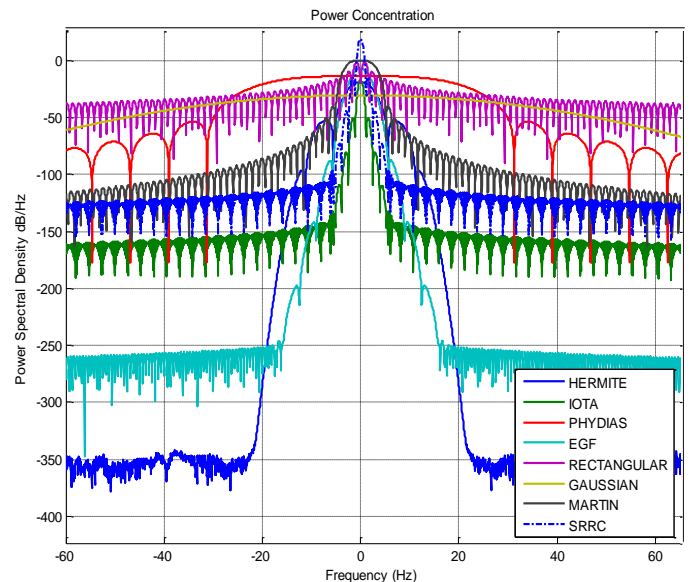


Fig. 3. Energy concentration.

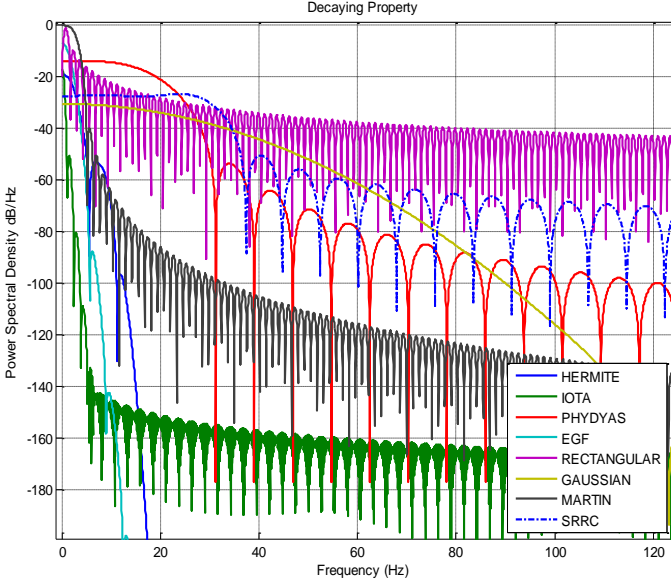


Fig. 4. Decaying property.

has the characteristic to improve the energy efficiency at the User Equipment (UE) through its low PAPR, this feature is due to an added stage of pre-coding (DFT) that is introduced in the OFDM chain (before IFFT). The linking between the DFT and IFFT stages can be regarded as a single carrier signaling that gets at lower PAPR by comparison to multi-carrier modulations. The CP-OFDM technique uses several sub-carriers to send a set of parallel low rate symbols. These complex symbols take values from a given constellation scheme. A cyclic prefix is added to each OFDM symbol as a guard

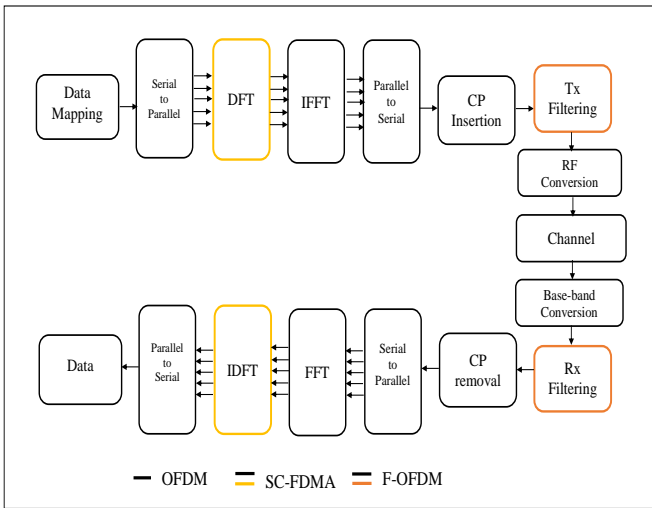


Fig. 5. CP-OFDM, SC-FDMA and F-OFDM transceivers.

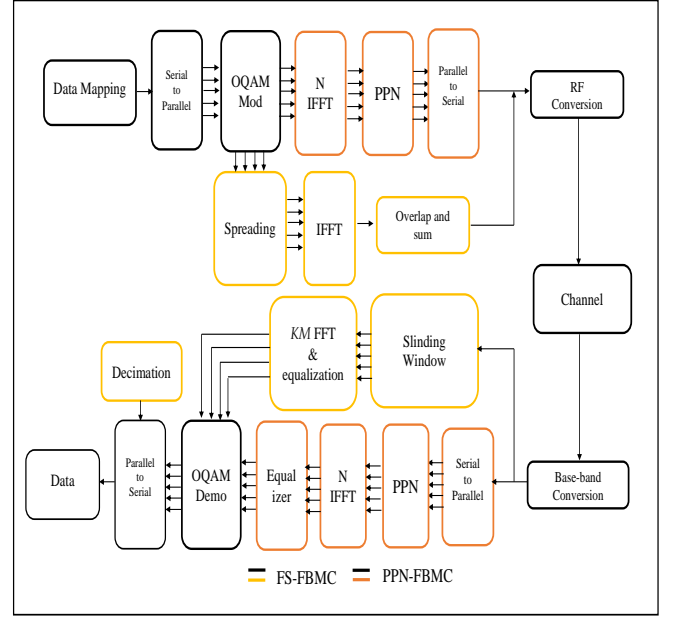


Fig. 6. PPN-FBMC and FS-FBMC transceivers.

interval to cope with the channel distortion. OFDM technique shows a low complexity in implementation, at the same time it achieves a good bandwidth efficiency. The simplicity of implementation is a consequence of the fact that each OFDM symbol is a sum of pure tones. Moreover, the equalization is ensured by only one tap equalizer. OFDM is no more available when the transmission is carried out on non-contiguous bands or when the channel is double dispersive. This because OFDM uses a square window in time domain and requires stringent time synchronization, its adoption in such environments has been found very difficult to set up. The time expression of the OFDM is given by equation (39) and the operating principle is shown in Fig.5.

$$x_{OFDM}(t) = \frac{1}{\sqrt{N}} \sum_{k=0}^{N-1} \left\{ x_k \times \Pi(t) \times e^{-i2\pi f_k t} \right\} \quad (39)$$

Where x_k denoted the complex symbols that emanate from a given constellation (e.g: QAM), $\Pi(t)$ denote the rectangular waveform filter and N the number of sub-carriers. This equation can be further developed to be :

$$= (-1)^n \times TFD^{-1} \left\{ x_k \sqrt{N} \right\}_{k=0}^{N-1} \quad (40)$$

B. FBMC

The filter bank multi-carrier (FBMC) modulation was first introduced by Chang [48] and Saltzberg [36]. The technique consists of filtering each sub-carrier at both emitter (synthesis filter) and receiver (analysis filter) in order to address the spectral OOB leakage of OFDM. The length of the prototype filter is generally K times the number of sub-carriers (size of the FFT), where K is the overlapping factor. Thus, each FBMC

symbol overlaps with K neighboring symbols in the time domain. The prototype filter must satisfy the Nyquist criterion to steer clear of the inter-symbol interference (ISI). The FBMC variants are [13]: Cosine modulated multi-tone scheme (CMT) where a set of pulse amplitude modulation (PAM) symbols are transmitted using vestigial side band (VSB) sub-carrier channels, the filtered multi-tone (FMT) based on complex QAM signaling and the staggered multi-tone scheme (SMT) based on double sideband (DSB) modulation, also referred to (FBMC/OQAM) for real valued offset QAM. Counter to FMT technique, FBMC-OQAM is able to achieve a maximum spectral efficiency (SE) due to its real orthogonality. So, OQAM does not exhibit any flaw compared to QAM since they achieve the same SE. Nevertheless, some techniques developed for CP-OFDM like pilot-based channel estimation and adaptation to Multiple-Input Multiple-Output (MIMO) systems are no more applicable to FBMC-OQAM. The FBMC structure can be efficiently implemented using IFFTs or FFTs combined with a polyphase network (PPN) [27] or using a frequency spreading (FS) approach [49] proposed recently as an alternative to PPN approach. The PPN-FBMC modulator shown in Fig.6, consists of an OQAM modulator, an IFFT of order N and polyphase networks bloc. The receiver applies a matched filter then performs an FFT of size N , the result feeds a multi-tap equalizer. In FS-FBMC (see Fig.6), OQAM symbols are filtered in frequency domain before the extended IFFT bloc by order KN . At the receiver side, a sliding window selects KN points every $N/2$ samples. Then, a FFT of size KM is applied followed by a filtering operation. The transmitted FBMC-OQAM signal is expressed as follows:

$$x_{FBMC}(t) = \sum_{k=0}^{K-1} \sum_{m=0}^{M-1} \left\{ d_{k,m} \theta_{k,m} \times g(n - mK/2) \times e^{\frac{j2\pi kn}{K}} \right\} \quad (41)$$

Where K and M are respectively the number of sub-carriers and the number of symbols, $d_{k,m}$ is the corresponding data symbol to be transmitted within the k^{th} frequency sub-carrier and the m^{th} time symbol, $g(n)$ refers to the prototype filter time coefficients (e.g.: IOTA[50], PHYDIAS[51], etc.). The $\theta_{k,m}$ term is defined as:

$$\theta_{k,m} = \begin{cases} \pm 1, & \text{if } m+k \text{ is even,} \\ \pm j, & \text{if } m+k \text{ is odd,} \end{cases} \quad (42)$$

A design and implementation of FBMC-OQAM transceiver on Field Programmable Gate Arrays (FPGA) logic device is presented in [52] and [53].

C. UFMC

Universal filtered multi-carrier (UFMC) technique can be considered a derivative of the OFDM with a sub-band filtering operation. This post-filtering process leads to a lower out-of-band leakage than for OFDM. The orthogonality between sub-carriers in each sub-band unit is maintained. Therefore UFMC can do without using offset mapping schemes like OQAM and by consequence can be used for MIMO systems. The

UFMC transmitter does not involve a cyclic prefix. However, a loss in spectral efficiency is noted due to the operation of linear convolution with the shaping filter (e.g., Dolph-Chebyshev filter)[54]. The length of the filter is timely short than FBMC one's, improving then the suitability of UFMC for short bursts of communication. Fig.7 shows the block diagram of an UFMC transceiver. In the T_x stage, the total bandwidth is splitted up to several sub-bands, each one containing a number of sub-carriers loading by QAM symbols. The result feeds an IDFT of size N followed by the filtering operation. The UFMC signal is obtained by the superposition of the sub-band-wise filtered components. The UFMC transmitter performs linear convolution of the IFFT output with a band-pass filter, but this implementation seems to be materially expensive. Another implementation method which reduces substantially the complexity consists of performing the filtering process in frequency domain [55]. The receiver stage is composed of a $2N$ point FFT, at the output of this block only even bins are considered to retrieve the data, the odd bins are loaded by inter-carrier interference (ICI) and they are not taken into consideration. Accordingly, a single tap equalizer is sufficient to recover the data. The discrete base-band UFMC signal is mathematically expressed as:

$$x_{UFMC}(n) = \sum_{k=0}^{K-1} S_k(n) * f_k(n) \quad (43)$$

Where K is the number of sub-bands, $f_k(n)$ represents the filter coefficients in sub-band of order k and $S_k(n)$ refers to the equivalent OFDM modulated signal over sub-band of order k expressed as:

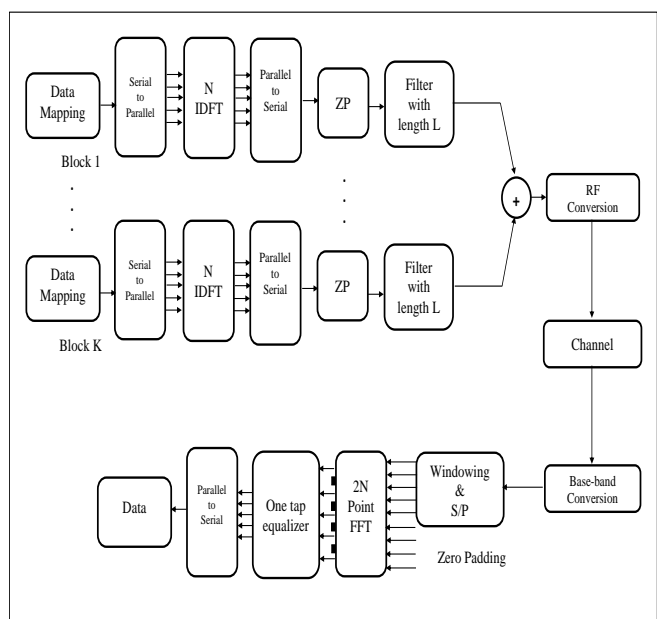


Fig. 7. UFMC transceiver.

$$S_k(n) = \sum_{m=0}^{M-1} s_{k,m}(n - m(N + N_g)) \quad (44)$$

The term M denotes the number of OFDM symbol blocks, and N_g is the length of the zero padding (ZP) added to each symbol.

$$s_{k,m}(n) = \sum_{l=(k-1)L}^{kL-1} A_{l,m,k} \times e^{j\frac{2\pi ln}{N}} \quad (45)$$

Where $A_{l,m,k}$ denotes the data (e.g: QAM symbols) transmitted over the l^{th} sub-carrier, the m^{th} temporal symbol block and the k^{th} sub-band. A reconfigurable architecture of UFMC with flexible numerology with its FPGA prototype extension is described in [56].

D. GFDM

The General frequency division multiplexing (GFDM) technique is a block-based techniques where data symbols are spread across two-dimensional structure (time and frequency). It transmits the data symbols during several times slots using different sub-carriers. This technique follows the same principle of FBMC by filtering each sub-carrier individually. A prototype filter is translated in time and frequency to filter each of $N = KM$ QAM complex symbols (one block) to be transmitted over K sub-carriers and M time slots. So by choosing a proper pulse shape, as root raised cosine (RRC) filter, we can ensure a low OOB emissions. This time-frequency filtering leads to a non-orthogonal waveform, but at the same time allows high-level of flexibility enabling GFDM to be used for sporadic communication [57]. To avoid the long filter tails of FBMC, GFDM filters each sub-carrier using a circular convolution operation with the RRC filter of length KM . The circular convolution process allows keeping the signal length unchanged before and after filtering. This circularity is also known as tail biting technique. A cyclic prefix is inserted in each block enabling GFDM to address the issue of inter-symbol interference. Thereby, GFDM reaches higher spectral efficiency than OFDM where CP is added to each symbol. The GFDM transceiver architecture is shown in Fig.8. In the T_x stage, the M QAM symbols to be transmitted in each sub-carrier are up-sampled by factor K , after that a convolution is performed with the circular time and frequency shifted version of the prototype filter, the outputs are then modulated with a sub-carrier center frequencies and superposed. This direct implementation seems to be potentially complex; a wisely reformulating of the GFDM transmitter based on IFFT/FFT approach saves considerably the complexity [58]. The GFDM receiver follows several architectures, namely the zero-forcing (ZF), matched filter (MF), and minimum mean square error (MMSE). The ZF receiver applies the inverse transmitting matrix to the received signal. The transmitting matrix contains operations of up-sampling, pulse shaping, sub-carrier up-conversion and superposition. For the case of the matched filter scheme, after the reception of the whole block, this one is filtered by the same translated filter used during

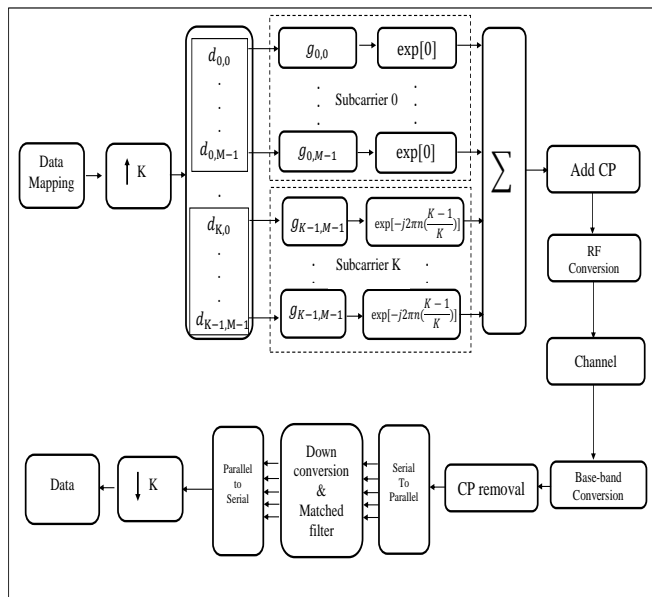


Fig. 8. GFDM transceiver.

the T_x stage. The MMSE technique attempts to counteract the noise amplification observed in ZF equalizers by balancing the variance of the noise samples and the data symbols [59]. The discrete GFDM signal carried by one block can be expressed as :

$$x_{GFDM}(n) = \sum_{k=0}^{K-1} \sum_{m=0}^{M-1} d_{k,m}(n) \times g_{k,m}(n), \quad 0 \leq n \leq KM - 1 \quad (46)$$

Where $d_{k,m}$ is the data symbol carried by k^{th} sub-carrier at m^{th} symbol and $g_{k,m}(n)$ is the circular shifted version of the prototype filter in time and frequency defined as:

$$g_{k,m}(n) = g((n - mK)_{KM}) e^{j\frac{2\pi kn}{K}}, \quad (47)$$

Where $g(n)$ is the prototype pulse shaping filter and the term $(\cdot)_{KM}$ is for the modulo operation of coefficient KM .

E. F-OFDM

Filtering is considered as a promising solution for reducing side lobes leakages. F-OFDM is one of techniques that introduce filtering operation to overcome the drawbacks of OFDM waveform. The F-OFDM technique is based either on a whole band filtering or a sub-band based splitting and filtering as with resource block F-OFDM (RB-F-OFDM) [60]. Two types of filters were considered for generating F-OFDM signal: In the case of the soft-truncated sinc filter, the sinc function is soft-truncated with different window functions, as a result the impulse response vanishes promptly and the ISI is circumscribed [61]. In the second type, the equiripple Filter structure uses the Remez algorithm associated with equiripple filters to get a sharper transition band so that to alleviate the inter sub-band interference [61].

TABLE III
PARAMETERS FOR THE WAVEFORMS SIMULATION.

General Parameters		OFDM	
Channel Bandwidth	10MHz	Occupied Subcarriers	600
Sub carrier spacing	15KHz	Guard Subcarriers	424
Sampling Frequency	15.36MHz	Symbol duration	66.67 us
Number of sub-carriers	1024	Number of Resource Blocks	50
Cyclic prefix length	72	Number of subcarrier per RB	12
bits Per SubCarrier	4		
FBMC		UFMC	
Overlapping factor	4	Guard interval length	72
Prototype filter	Phydias	Sub-band width	12
Filter length	4096	Chebyshev filter length	73
Number of Resource Blocks	50	Side-lobe attenuation	40dB
GFDM		F-OFDM	
GFDM block length	15	Filter length	513
Number of guard symbols	2	Number of RB	50
Receiver type	MF	Number of SCs in 1 RBs	12
RRC filter roll-off	0.2	Tone offset	2.5
Number of IC iterations	4	Filter type	Windowed Sinc (RRC)

TABLE IV
WAVEFORMS SPECTRAL EFFICIENCY.

Waveform	Time Overhead (T_G)	Guard band (N_G)	Time efficiency $TE(M = 1)$	Frequency efficiency $FE (M = 1)$	Spectral efficiency $SE (M = 1)$
OFDM	$M \times T_{CP}$	6M	0.8928	0.9009	0.8043
FBMC	$N \times (K - 1/2)$	2M	0.2808	0.9966	0.2799
UFMC	$M (T_{ZP} + (L_{UFMC} - 1))$	2M	0.8064	0.9966	0.8036
GFDM	$\frac{M}{N_B} (N_B T_{GS} + T_{CP})$	2M	0.9937	0.9966	0.9903
F-OFDM	$M \times T_{CP}$	6M	0.8928	0.9009	0.8043

The F-OFDM filter length is relatively short and the sub-carriers are quasi orthogonal by comparison to GFDM waveform. Fig.5 depicts the F-OFDM transceiver. The system is based on an OFDM structure. The transmitter generates the OFDM signal based on the N -Point IFFT and a CP insertion blocks. The F-OFDM signal is then obtained by passing the result through an appropriately designed spectrum shaping filter. At the R_X side, the received signal is first passed through a matched filter block and then the resulting signal feeds a regular OFDM receiver. The F-OFDM signal can be expressed as:

$$x_{F-OFDM}(t) = x_{OFDM}(t) * F(t) \quad (48)$$

Where $F(t)$ is the used shaping filter.

V. PERFORMANCE COMPARISON

This section is dedicated to the comparison between the filtered waveforms. The comparison is based on several key performance indicators. These are representative for the selection between waveform candidates. The performance of the different waveforms is assessed in terms of their potential to fill the major requirements of new communication networks. The simulation parameters are taken under the LTE specifications [62]. These ones are listed in Table.III.

A. Power Spectral Density

The power spectral density (PSD) describes how the power of a signal is distributed in frequency range. It is an important factor that indicates the OOB radiation's level and the ability of a given waveform to reuse the spectrum and to support coexistence of different services. Therefore, a lower OOB enables users to access network in an asynchronous mode and to incarnate a high mobility. The different PSDs are depicted in Fig.9. The FBMC-OQAM waveform with an overlapping factor $K = 4$ represents the best spectral localization. For short burst transmission, a lower pulse duration can be obtained by reducing the overlapping factor K of the prototype filter. However, the spectral containment of the FBMC-OQAM is less efficient as the K factor decreases.

Indeed, the OOB of the FBMC-OQAM is 126dB, 116dB and 8dB lower than the OFDM one for an overlapping factor $K = 4$, $K = 3$ and $K = 2$ respectively. The recent work [63] introduces a new prototype filter design for FBMC-OQAM based on convex optimization. It is capable to supply a high symbol reconstruction with best spectral feature. GFDM has a slightly lower out-of-band leakage compared to OFDM (about 12dB) but it is clearly outperformed by UFMC.

The OOB for GFDM can be reduced further by using a windowing operation, hereby it approaches UFMC performances. In [64] the flexibility of the GFDM transmit matrix is examined in order to generate a linear GFDM waveform where good spectral containment of FBMC is achieved. The UFMC technique filters each block separately and as a result has a lower OOB leakage compared to OFDM, but it is outperformed by FBMC-OQAM where the filtering is applied to each sub-carrier. As for the F-OFDM, there is one filter

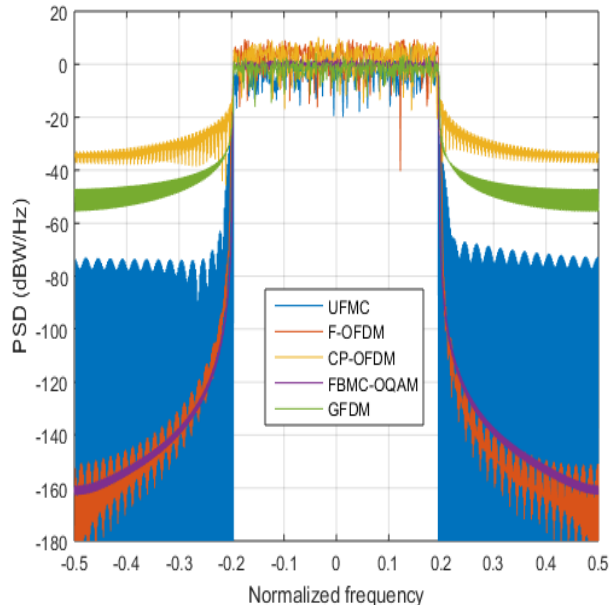


Fig. 9. Power spectral density.

applied on the whole bands which reduce considerably the OOB. From Fig.9, one can grasp that OFDM owns the worst PSD. To deal with, a spectral encapsulation is introduced in [65] to shape the spectrum of OFDM.

B. Spectral Efficiency

The spectral efficiency parameter represents the number of bits transmitted over a time-frequency unit. This parameter is the product of the time efficiency (TE) and frequency efficiency (FE). The frequency efficiency characterizes the localization and the spectrum containment of a given waveform in the frequency domain, while the time efficiency quantifies the time overhead introduced to the data symbol. The frequency efficiency depends on the number of active sub-carriers and the number of guard sub-carriers. The time efficiency is function of the number of samples of symbols in a data burst and the number of overhead samples (CP, filter tail or pilot symbols, etc.). The spectral efficiency represents a key parameter to assess the performance of modulation schemes, it is defined by [26]:

$$SE = \frac{N_D}{N_D + N_G} \times \frac{T_D}{T_D + T_G} \quad (49)$$

Where N_D and N_G are respectively the number of data sub-carriers (600 in LTE) and guard band sub-carriers, on the other hand, T_D and T_G represent the data and time overhead samples. The TE, FE and related SE for each waveform are summarized in Table.IV for M multi-carrier symbols. The CP inserted in OFDM and F-OFDM constitutes the only overhead samples. The Time-domain overhead for OFDM and F-OFDM is proportional to CP and burst length, thus their time efficiency is depending only on CP length. The FBMC system incurs an overhead due to the filter tails and

time offset between the OQAM symbols. It uses inefficiency spectral resources because of these long ramp-up and ramp-down tails especially for short bursts. A novel method for shortening these tails is set forth in [66] and therefore improving spectral efficiency. The time efficiency in FBMC-OQAM is independent from the frame size. GFDM represents the highest efficiency due to its block-based feature using a unique CP per frame. Otherwise, UFMC introduces a filter tail in each block and has an overhead equals to the summation of the filter length and the zero padding samples. According to the LTE standard, 666 sub-carriers of 15KHz wide fit the 10MHz bandwidth and the number of sub-carriers carrying data is 600. The FBMC-OQAM,GFDM and UFMC are designed to achieve a narrow OOB radiation and thus require few guard bands (one on each side). OFDM and F-OFDM do not exhibit very low OOB, in these two cases, the guard band is expected to be more large. Fig.10 evinces that all waveforms exhibit a constant spectral efficiency versus the number of multicarrier symbols except the FBMC-OQAM, this one depends on the frame duration and its performance approaches that of the UFMC as the number of symbols per frame increases. GFDM is the most spectral efficiency waveform thanks to it well frequency localization and thanks to the tail biting technique. Due to the constant filter tails, UFMC shows a time efficiency that approaches that of the OFDM with a slight improvement due to lower guard band required for UFMC. F-OFDM and OFDM show the same performances since using hard truncation.

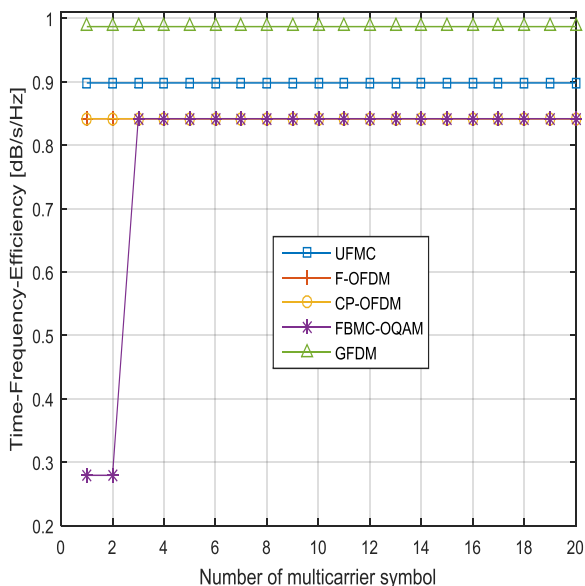


Fig. 10. Spectral efficiency.

C. Bit Error Rate

The performance of the considered waveforms in terms of bit error rate (BER) is assessed using the Extended Vehicular A channel model (EVA) defining a medium delay spread

environment. The EVA channel model represents a multi-path delay profile used to measure performance in multi-path fading environment. A multi-path fading propagation conditions are defined by a combination of a multi-path delay profile (EVA) and a large Doppler frequency. Here we set the Doppler frequency to 5 Hz. Fig.11 shows the BER versus SNR for the EVA channel. We assume for the simulation that the channel state information (CSI) is perfectly known and no synchronization misalignment is considered. The receiver uses a hard decision. Thanks to the samples of the CP guard interval, the CP-OFDM and F-OFDM implementations show an excellent performance. The FBMC-OQAM due to the long filter length outperform GFDM performance. Decreasing the size of FFT block in the FBMC-OQAM implementation degrades the performance in terms of BER, this is mainly caused by the resulting reducing in the filter length in the time domain. In this moderately frequency selective channel, CP-OFDM and UFMC do likewise. GFDM implementation exhibits the worse BER compared to other waveforms. The BER level seems to reach high-level with high constellation order for all considered waveforms. In[67] local discrete Gabor transform (LDGT) algorithm is used with a new type of prototype filter to eliminate interference in GFDM system. The proposed filtering introduces the orthogonality condition and have separate filters for the even and odd subcarriers respectively.

D. Energy Efficiency

Information and communication technology industries are contributing more and more to the CO₂ emission because of their high energy consumption. This energy is used to serve the great demand on electricity, especially by the base station (BS) [68]. Therefore, one of the main challenges of 5G and B5G communication systems is to enhance their energy efficiency.

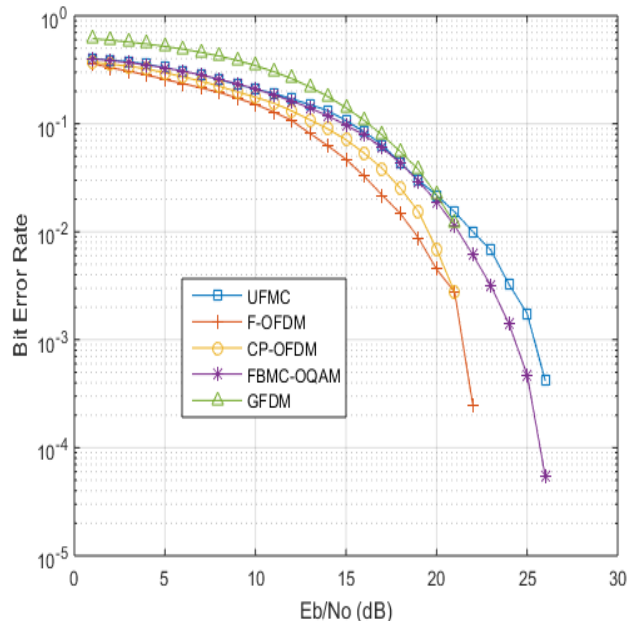


Fig. 11. Bit error rate.

The peak-to-average power ratio (PAPR) is a critical parameter for describing waveforms energy efficiency. Waveforms having high PAPR limit the Power amplifier (PA) to operate in its linear region. This restraint reduces significantly Power amplifier efficiency (PAE). Contrarily, waveforms with low PAPR allow PA to operate near saturation region, reaching thus high efficiency. PAPR represents the ratio of the peak power of the signal to its average power. The PAPR is defined as :

$$PAPR = \frac{Max|x(t)|^2}{E[|x(t)|^2]} \quad (50)$$

Since PAPR is viewed as a random variable, the PAPR description of the filtered waveforms is provided by the complementary cumulative distribution function (CCDF). This one is defined for a threshold γ by:

$$CCDF_{PAPR} = Pr_{\gamma}(PAPR > \gamma) \quad (51)$$

We compute on Fig.12, the CCDF of the PAPR for each waveform. The filtered waveforms show all a high PAPR, this is due to their multi-carrier nature. The OFDM waveform detains the best performance, while F-OFDM shows the highest PAPR about 1dB compared to OFDM. The Filtering operation used in F-OFDM is the major contributors to PAPR increase. FBMC-OQAM, GFDM and UFMC even they show a high PAPR than OFDM (0.4dB), they remain slightly better than F-OFDM. Several PAPR reduction techniques have been proposed to deal with the high PAPR of multi-carrier systems. Distorting the signal before the amplification processing can reduce PAPR, clipping and filtering [69], peak windowing [70] and companding [71] belong to the signal distortion techniques class. Other techniques generate multiple permutations of the multi-carrier signal. They transmit the one with minimum PAPR or modify the signal parameters like the phase or constellation to achieve a low PAPR. These techniques like Tone reservation (TR)[72], Tone injection [72] and Partial Transmit Sequence (PTS) [73] are called Probabilistic Techniques. There is a third class based on coding the signal sequences, this one is called coding techniques class. The all mentioned techniques are well established for OFDM systems, but not yet completely investigated for the other considered waveforms.

E. Complexity

The computational complexity for a given waveform is a key parameter to assess how they can be executed by processors. The presented complexity is only a fraction of the overall system complexity, RF digital pre-processing and encoders consume a lot of operations as well. The complexity is evaluated in terms of the number of real multiplications per multi-carrier symbol. This one is used as a metric for modulator complexity. The transceiver complexity of the different waveforms are summarized in Table.V. The values in Table.V don't take the complexity of the equalizer into account. For CP-OFDM system, the required complexity to generate the

signal is reduced to the IFFT block operation at the transmitter and to an FFT block operation at the receiver. If we do not take in consideration the complexity of the equalizer, the complexity of OFDM transmitter/receiver only equals the number of real multiplications in IFFT/FFT stages. Thus, the OFDM transceiver complexity is the double of one stage. OFDM represents the lowest computational complexity between all waveforms. The split-radix algorithm is considered for the IFFT and FFT implementation. The FBMC technique controls the frequency response by introducing a filter bank centered on the active sub-carriers and based on the same prototype filter. For the poly-phase decomposition structure, an efficient implementation is obtained by deploying an offset-QAM staggering, a phase rotation for linear phase, an IFFT/FFT and a poly-phase filtering [74]. The FFT block in transmitter side is fed with pure real or imaginary symbols (OQAM symbols) which result in less complexity. However, the receiver FFT block uses complex inputs/outputs symbols. FBMC technique is nearly six times more complicated than OFDM. A straightforward implementation of the UFMC technique in frequency domain consists of summing up all sub-bands with per sub-band operations of IFFT and filtering, but this direct implementation is not efficient. An efficient implementation method of the UFMC modulator is proposed in [75] using overlapping sub-bands. Each sub-band is proceeded by small size IFFT/FFT, the filtering operation is performed in the frequency domain and the overlapping sub-bands are superimposed in a large $2N$ -IFFT block, in which the number 2 represents the oversampling factor. Each sub-band requires an IFFT of size N and an FFT of size $2N$. The frequency filtering operation requires $8N$ real multiplications. The R_x stage includes a windowing in the time domain, FFT block of size $2N$ with zero padding and a frequency domain filtering. With this

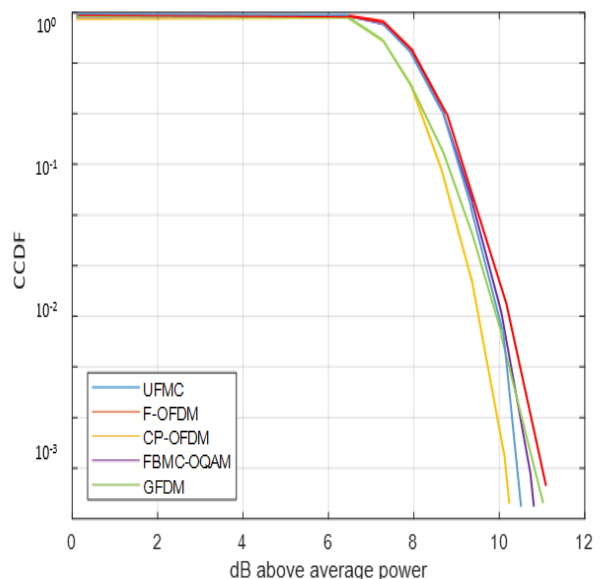


Fig. 12. Complementary cumulative distribution function.

structure, UFMC generates the highest complexity compared to the other waveforms. The GFDM technique is based on a two-dimensional data structure, data symbols are grouped in blocks containing each one N sub-carriers and M time slots. The processing of these blocks is based on digital filters with tail-biting property that preserves circular properties across frequency and time domain. The generation of GFDM signal requires a domain conversion in which data signal of each sub-carrier is converted into the frequency domain. Then, after an up-sampling operation, a filtering process is applied in the frequency domain followed by a frequency up-conversion. Finally, the signal is re-transformed into the time domain [76]. The receiver contains transformation of the signal into the frequency domain, a frequency filtering and a re-transformation to time domain [76]. A recent low complexity modem design for GFDM waveform is proposed in [59]. Due to the circular filtering, GFDM is far less complex than UFMC. The Filtered OFDM aims to improve the spectral containment of the traditional CP-OFDM using a filter at the output of a CP-OFDM transmitter. In addition to the IFFT block, the complexity of F-OFDM system entails more terms induced by the filtering operation. The used filter is real and the filtering operation is followed by an up-conversion that contribute to the complexity with an extra real multiplication [77]. In [78], singular value decomposition based F-OFDM (SF-OFDM) system is proposed with much short filter length than F-OFDM system. This approach reduces considerably the burden of the F-OFDM system.

F. Resilience to PA non-linearity

Power amplifiers (PA) play a key role in both transmitter and receiver sides of a communication system. They bring the desired signal to a suitable level of transmission or for demodulation. PAs introduce two main impairments due to their non ideal nature: nonlinearity and additive noise. The power amplifier is the most frequent source of non-linearity in the transmitter. The nonlinear behavior of an amplifier can be described in a general manner by a power series expansion [79]. The nonlinear feature of PAs introduces both an out-of-band spectral regrowth and in-band distortion. The in-band interference is usually characterized by the error vector magnitude (EVM). The spectral regrowth comes especially from the convolution operation involved in the Fourier transform expression of the non-linearity model. The robustness to PA non-linear distortions is assessed using the output back-off (OBO) parameter. To check the resilience of filtered waveforms to PA non-linearity, we use the Saleh model and the modified Rapp model. The Saleh model has the following amplitude (AM-AM) and phase (AM-PM) characteristics [80]:

$$f_{S_{AM/AM}}(x) = \frac{A \cdot x}{1 + B \cdot x^2} \quad (52)$$

$$f_{S_{AM/PM}}(x) = \frac{C \cdot x^2}{1 + D \cdot x^2} \quad (53)$$

Where x denotes the amplitude of the input signal and A, B, C, D are PA parameters. The Rapp model is based on

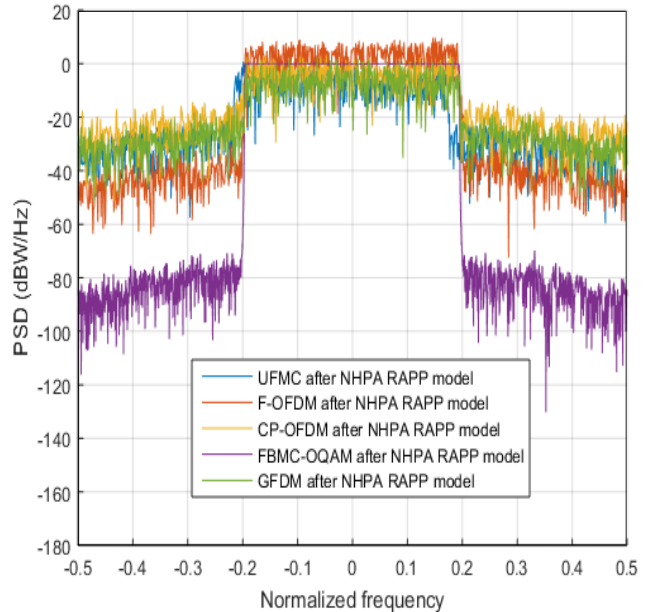


Fig. 13. Nonlinear Power amplifier effect.

experimental measurements with an AM-AM and AM-PM characteristics given by [80]:

$$f_{R_{AM/AM}}(x) = \frac{G \cdot x}{\left(1 + \left(\frac{G \cdot x}{V_{SAT}}\right)^{2P}\right)^{\frac{1}{2P}}} \quad (54)$$

$$f_{R_{AM/PM}}(x) = 1 \quad (55)$$

The AM/AM and AM/PM characteristics describe how the instantaneous input amplitude influences the output amplitude and phase, respectively. The spectral regrowth of the different filtered waveforms due to Power amplification operation are depicted in Fig.13 for the modified Rapp models. It is clear that the type of the model affects the OOB spectral regrowth level of the waveform passing through the PA. This out-of-band distortion can significantly reduce the system performances in a multi-users access configuration. The out-of-band distortions are investigated by calculating the adjacent channel power ratio (ACPR). The results are shown in Fig.14. The in-band distortion are measured using the error vector magnitude. The EVM is defined as the normalized magnitude of the difference between the input and output of a non-linearity. It measures the extent of the departure of the signal constellation from the ideal reference. The constellation mapping or BER are also used as in-band distortion indicators (Fig.11).

VI. FILTER-WAVEFORM DEPENDENCY

The present review deduces the strong relationship between the prototype filter properties and the corresponding filtered waveform performances. The filtering operation, as first goal, tends to enhance the spectrum containment. This alleviates the abundant use of the spectrum and allows coexistence between systems by enhancing PSDs and reducing OOB leakage.

TABLE V
WAVEFORMS COMPLEXITY.

T_x Complexity	Waveform	R_x Complexity
	CP-OFDM	
$C_{IFFT} = N \log_2 N - 3N + 4$		$C_{FFT} = N \log_2 N - 3N + 4$
	FBMC-OQAM (PPN)	
$C_{SFB} = N(\log_2(\frac{N}{2}) - 3) + 8 + 4(NK + 1)$		$C_{AFB} = 2N(\log_2(N) - 3) + 8 + 4(NK + 1)$
	UFMC	
$B[C_{IFFT}(N) + C_{FFT}(2N) + 8N] + C_{FFT}(2N)$		$C_{FFT}(2N) + 8N$
	GFDM	
$NM \log_2(M) + NLM + MN \log_2(MN)$		$NM \log_2(NM) + NLM + NM \log_2(M)$
	F-OFDM	
$2N \log_2 N - 6N + 8 + 2(N + T_{CP})L_F + 2NL_F$		$2N \log_2 N - 6N + 8 + 2(N + T_{CP})L_F + 2NL_F$

TABLE VI
PAPERS DEALING WITH FILTERED WAVEFORMS.

Waveform	OFDM	FBMC	UFMC	GFDM	F-OFDM
Channel Estimation	[122],[123] [124],[125]	[143],[144]	[153],[154]	[164],[165] [166]	[181]
Equalization	[126],[127] [128],[129]	[100],[145]	[155],[156]	[167],[168] [169]	[182]
Synchronization	[130], [131] [132]	[83], [146]	[157], [158]	[170], [171] [172]	
PAPR	[133],[134] [135], [136]	[135],[147] [148]	[159],[185]	[173],[174] [175]	[183]
MIMO compatibility	[137],[138] [139]	[149], [150]	[160], [161]	[176], [177] [178]	
Resource Allocation	[140], [141] [142]	[151], [152]	[162], [163]	[179], [180]	[184]

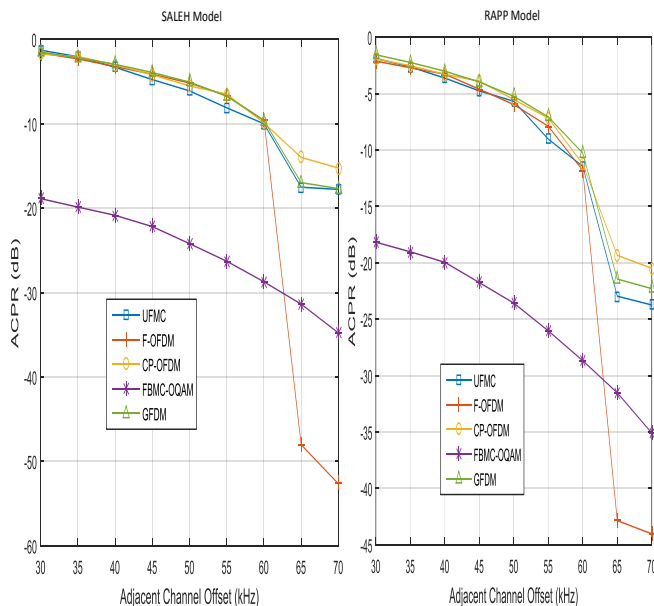


Fig. 14. Adjacent channel power ratio.

The filter decaying property and ambiguity function are in control of these characteristics. Additionally, filtering operation augments the frequency localization and reduces ICI and ISI. The complexity of a given waveform depends directly on the length of the filter and the number of filter taps. The time domain implementation is generally more complex than in frequency domain. The waveform latency systematically depends on the length of the filter. Good latency can be achieved through a good time localization of the filter. However, in some cases, the need for a long filter is to avoid ISI and ICI. The circular convolution and oversampling process also alter the latency performance [81]. The prototype filter affects the spectral efficiency performance as well. A well time-frequency localized pulse shape filter makes the waveform more suitable for a good spectral efficiency. However the length of the filter and its stopband attenuation can result in a reduction of the spectral efficiency. As for PAPR, the prototype filter length has a significant influence on the probability distribution of the PAPR and on the PAPR reduction technique. For example the PAPR increases when the symbols overlap becomes significant due to long prototype filter in the case of FBMC. So, according to this survey, a key element to be undertaken in the design of the 5G and B5G systems is the close relationship between the prototype filters and the performances of the resulting filtered waveforms. These performance parameters can be formulated as typical filter design problematic or as a filter coefficient optimization problem as in [82].

VII. CONCLUSION

Due to the diverse applications of new communication networks, the architectural adjustments associated with the radio access layer seem to be mandatory. These ones extend from including new air-interfaces to deployment of new multiple access techniques for heterogeneous networks. The

design of prototype filters constitutes an arresting step for the conception of new air-interfaces like filtered and bank filtered ones. These modulations schemes are based on a number of contiguous and frequency translated bands conceived from the same prototype filter. The ambiguity function represents an important factor used to compare and to differentiate between prototype filter's efficiency in terms of ISI and ICI free transmission. Filters covered here are designed to satisfy a good time/frequency localization and a near perfect orthogonality. Energy concentration and transition band decay are other important selecting criteria that indicated how the energy is distributed and how fast is the filter transition band slope. These factors are important in determining the spectral regrowth in presence of radio front-end impairments and systems coexistence leakage. The review found that the prototype filter properties (length, transition band,...) affect the performance of the filtered waveforms. The study approves its usefulness in determining the overall complexity, latency, spectral efficiency and BER. Although most filters show good performances, the choice depends on practical concerns as implementation and numerical complexity. Also, new air-interface waveforms have been extensively analyzed and evaluated based on several key performance indicators. Power spectral density, spectral efficiency, BER, PAPR and computational complexity and resistance to PA impairment have been assessed. It is clear from the comparison that all considered waveforms drastically improve the PSD with respect to OFDM. Since all waveforms are multi-carrier schemes, they all have the same PAPR issue. Recently Energy Harvesting and artificial intelligence-based solutions have been proposed to alleviate this problem. The F-OFDM and UFMC are interesting options to replace OFDM as they enhance performance in terms of PSD and of asynchronous access. Furthermore, these waveforms are compatible to almost OFDM algorithms (channel estimation, equalization and spatial diversity). The energy efficiency and weak resilience to PA impairment stay the main drawbacks for UFMC and F-OFDM waveforms. Presenting the best time-frequency containment entitling the use of fragmented spectrum and energy efficiency comparable to that of OFDM ; GFDM and FBMC-OQAM are also high attractive candidates. Even if the FBMC-OQAM exhibits good performance in non-synchronous access, it is not adapted to short packet size. GFDM implementation represent the best performance in terms of SE. However, due to the lack of orthogonality, this waveform had difficulty finding MIMO compatibility. MIMO and massive MIMO ability is an open problem for multicarrier non-orthogonal waveforms. Still, there is a tremendous amount of research in this field and early results show that all candidate waveforms have a potential to be implemented with MIMO systems. The multi-numerology concept, where multiple frame structures with different sub-carrier spacing coexist, is a new research direction in this field. Various critical issues concerning multi-numerology system have emerged such as: inter-numerology interference and orthogonality between sub-carriers of different numerologies. GFDM and FBMC-OQAM incarnate a high complexity. This one is still a high topic for these two waveforms. Finally, it seems that there is no definite preferable modulation format. Even if OFDM has

been nominated for 5G standard because of its implementation simplicity, the choice will depend essentially on the considered scenarios and the selected parameters, leaving the field open for future proposals and contributions.

REFERENCES

- [1] Fayeze Ghavimi and Hsiao-Hwa Chen. M2m communications in 3gpp lte/lte-a networks: Architectures, service requirements, challenges, and applications. *IEEE Communications Surveys & Tutorials*, 17(2):525–549, 2014.
- [2] Charith Perera, Arkady Zaslavsky, Peter Christen, and Dimitrios Georgakopoulos. Context aware computing for the internet of things: A survey. *IEEE communications surveys & tutorials*, 16(1):414–454, 2013.
- [3] Arash Asadi, Qing Wang, and Vincenzo Mancuso. A survey on device-to-device communication in cellular networks. *IEEE Communications Surveys & Tutorials*, 16(4):1801–1819, 2014.
- [4] Manuel Eugenio Morocho-Cayamcela, Haeyoung Lee, and Wansu Lim. Machine learning for 5g/b5g mobile and wireless communications: Potential, limitations, and future directions. *IEEE Access*, 7:137184–137206, 2019.
- [5] Thomas Strohmer and Scott Beaver. Optimal ofdm design for time-frequency dispersive channels. *IEEE Transactions on communications*, 51(7):1111–1122, 2003.
- [6] Henry J Landau and Henry O Pollak. Prolate spheroidal wave functions, fourier analysis and uncertainty—ii. *Bell System Technical Journal*, 40(1):65–84, 1961.
- [7] Kenneth W Martin. Small side-lobe filter design for multitone data-communication applications. *IEEE Transactions on Circuits and Systems II: Analog and Digital Signal Processing*, 45(8):1155–1161, 1998.
- [8] Ralf Haas and Jean-Claude Belfiore. A time-frequency well-localized pulse for multiple carrier transmission. *Wireless personal communications*, 5(1):1–18, 1997.
- [9] Yangyang Guan, Yongle Wu, and Manos M Tentzeris. A bidirectional absorptive common-mode filter based on interdigitated microstrip coupled lines for 5g “green” communications. *IEEE Access*, 8:20759–20769, 2020.
- [10] Robert Vallet and Kais Haj Taieb. Fraction spaced multi-carrier modulation. *Wireless personal communications*, 2(1-2):97–103, 1995.
- [11] G Walter and T Soleski. A new friendly method of computing prolate spheroidal wave functions and wavelets. *Applied and Computational Harmonic Analysis*, 19(3):432–443, 2005.
- [12] Ian C Moore and Michael Cada. Prolate spheroidal wave functions, an introduction to the slepian series and its properties. *Applied and Computational Harmonic Analysis*, 16(3):208–230, 2004.
- [13] Behrouz Farhang-Boroujeny and ChungHim Yuen. Cosine modulated and offset qam filter bank multicarrier techniques: a continuous-time prospect. *EURASIP Journal on Advances in Signal Processing*, 2010:1–16, 2010.
- [14] Pierre Siohan, Cyrille Siclet, and Nicolas Lacaille. Analysis and design of ofdm/oqam systems based on filterbank theory. *IEEE transactions on signal processing*, 50(5):1170–1183, 2002.
- [15] Bernard Le Floch, Michel Alard, and Claude Berrou. Coded orthogonal frequency division multiplex [tv broadcasting]. *Proceedings of the IEEE*, 83(6):982–996, 1995.
- [16] Richard J Duffin and Albert C Schaeffer. A class of nonharmonic fourier series. *Transactions of the American Mathematical Society*, 72(2):341–366, 1952.
- [17] Christian Roche and Pierre Siohan. A family of extended gaussian functions with a nearly optimal localization property. In *Multi-carrier spread-spectrum*, pages 179–186. Springer, 1997.
- [18] Shahriar Mirabbasi and Ken Martin. Design of prototype filter for near-perfect-reconstruction overlapped complex-modulated transmultiplexers. In *2002 IEEE International Symposium on Circuits and Systems. Proceedings (Cat. No. 02CH37353)*, volume 1, pages I–I. IEEE, 2002.
- [19] Miquel Payaró, Antonio Pascual-Iserte, Ana Garcia-Armada, and Matilde Sánchez-Fernández. Resource allocation in multi-antenna mac networks: Fbmc vs ofdm. In *2011 IEEE 73rd Vehicular Technology Conference (VTC Spring)*, pages 1–5. IEEE, 2011.
- [20] Richard van Nee and Ramjee Prasad. *OFDM for wireless multimedia communications*. Artech House, Inc., 2000.
- [21] Behrouz Farhang-Boroujeny. Ofdm versus filter bank multicarrier. *IEEE signal processing magazine*, 28(3):92–112, 2011.
- [22] Lerry Bayunuari Nugraha and Effrina Yanti Hamid. Performance comparison of pilot aided channel estimation in smt-fbmc and ofdm. In *2016 10th International Conference on Telecommunication Systems Services and Applications (TSSA)*, pages 1–5. IEEE, 2016.
- [23] Kilbom Lee, Sang-Rim Lee, Sung-Hyun Moon, and Inkyu Lee. Mmse-based cfo compensation for uplink ofdma systems with conjugate gradient. *IEEE Transactions on Wireless Communications*, 11(8):2767–2775, 2012.
- [24] Kilbom Lee and Inkyu Lee. Cfo compensation for uplink ofdma systems with conjugated gradient. In *2011 IEEE International Conference on Communications (ICC)*, pages 1–5. IEEE, 2011.
- [25] Xiaojing Huang, Jian A Zhang, and Y Jay Guo. Out-of-band emission reduction and a unified framework for precoded ofdm. *IEEE Communications Magazine*, 53(6):151–159, 2015.
- [26] Frank Schaich and Thorsten Wild. Waveform contenders for 5g—ofdm vs. fbmc vs. ufmc. In *2014 6th international symposium on communications, control and signal processing (ISCCSP)*, pages 457–460. IEEE, 2014.
- [27] Maurice Bellanger, D Le Ruyet, D Roviras, M Terré, J Nossek, L Baltar, Q Bai, D Waldhauser, M Renfors, T Ihalainen, et al. Fbmc physical layer: a primer.

- Phydyas*, 25(4):7–10, 2010.
- [28] Ari Viholainen, Tero Ihalainen, Tobias Hidalgo Stitz, Markku Renfors, and Maurice Bellanger. Prototype filter design for filter bank based multicarrier transmission. In *2009 17th European Signal Processing Conference*, pages 1359–1363. IEEE, 2009.
- [29] Maurice G Bellanger. Specification and design of a prototype filter for filter bank based multicarrier transmission. In *2001 IEEE International Conference on Acoustics, Speech, and Signal Processing. Proceedings (Cat. No. 01CH37221)*, volume 4, pages 2417–2420. IEEE, 2001.
- [30] SMJ Asgari Tabatabaee and Hossein Zamiri-Jafarian. Prototype filter design for fbmc systems via evolutionary pso algorithm in highly doubly dispersive channels. *Transactions on Emerging Telecommunications Technologies*, 28(4):e3048, 2017.
- [31] Haijian Zhang, Didier Le Ruyet, Daniel Roviras, and Hong Sun. Polyphase filter bank based multi-band spectrum sensing in cognitive radio systems. *International Journal of Communication Systems*, 29(12):1844–1862, 2016.
- [32] Nicola Michailow, Maximilian Matthé, Ivan Simões Gaspar, Ainoa Navarro Caldevilla, Luciano Leonel Mendes, Andreas Festag, and Gerhard Fettweis. Generalized frequency division multiplexing for 5th generation cellular networks. *IEEE Transactions on Communications*, 62(9):3045–3061, 2014.
- [33] Vida Vakilian, Thorsten Wild, Frank Schaich, Stephan ten Brink, and Jean-François Frigon. Universal-filtered multi-carrier technique for wireless systems beyond lte. In *2013 IEEE Globecom Workshops (GC Wkshps)*, pages 223–228. IEEE, 2013.
- [34] Pei Xiao, Ciaran Toal, Dwayne Burns, Vicent Fusco, and Colin Cowan. Transmit and receive filter design for ofdm based wlan systems. In *International Conference on Wireless Communications and Signal Processing (WCSP), 2010*, 2010.
- [35] Erdem Bala, Jialing Li, and Rui Yang. Shaping spectral leakage: A novel low-complexity transceiver architecture for cognitive radio. *IEEE Vehicular Technology Magazine*, 8(3):38–46, 2013.
- [36] B Saltzberg. Performance of an efficient parallel data transmission system. *IEEE Transactions on Communication Technology*, 15(6):805–811, 1967.
- [37] Malte Schellmann, Zhao Zhao, Hao Lin, Pierre Siohan, Nandana Rajatheva, Volker Luecken, and Aamir Ishaque. Fbmc-based air interface for 5g mobile: Challenges and proposed solutions. In *2014 9th international conference on cognitive radio oriented wireless networks and communications (CROWNCOM)*, pages 102–107. IEEE, 2014.
- [38] Ronald Newbold Bracewell and Ronald N Bracewell. *The Fourier transform and its applications*, volume 31999. McGraw-Hill New York, 1986.
- [39] John G Proakis and Dimitris G Manolakis. *Digital communications*, volume 4. McGraw-hill New York, 2013.
- [40] Ken Gentile. Digital pulse-shaping filter basics. *Application Note AN-922. Analog Devices, Inc.(September)*, 2007.
- [41] Michael Joost. Theory of root-raised cosine filter. *Research and Development*, 47829, 2010.
- [42] Ralf Haas and J-C Belfiore. Multiple carrier transmission with time-frequency well-localized impulses. In *IEEE Second Symposium on Communications and Vehicular Technology in the Benelux*, pages 187–193. IEEE, 1994.
- [43] Jinfeng Du and Svante Signell. Classic ofdm systems and pulse shaping ofdm/oqam systems, 2007.
- [44] Pierre Siohan and Christian Roche. Cosine-modulated filterbanks based on extended gaussian functions. *IEEE Transactions on signal processing*, 48(11):3052–3061, 2000.
- [45] Seymour Stein. Algorithms for ambiguity function processing. *IEEE Transactions on Acoustics, Speech, and Signal Processing*, 29(3):588–599, 1981.
- [46] Fredric J Harris. On the use of windows for harmonic analysis with the discrete fourier transform. *Proceedings of the IEEE*, 66(1):51–83, 1978.
- [47] Puneet Singla and Tarunraj Singh. Desired order continuous polynomial time window functions for harmonic analysis. *IEEE Transactions on Instrumentation and Measurement*, 59(9):2475–2481, 2009.
- [48] Robert W Chang. Synthesis of band-limited orthogonal signals for multichannel data transmission. *Bell System Technical Journal*, 45(10):1775–1796, 1966.
- [49] Maurice Bellanger. Fs-fbmc: An alternative scheme for filter bank based multicarrier transmission. In *2012 5th international symposium on communications, control and signal processing*, pages 1–4. IEEE, 2012.
- [50] Shahid Mehmood, Deepak Dasalukunte, and Viktor Owall. Hardware architecture of iota pulse shaping filters for multicarrier systems. *IEEE Transactions on Circuits and Systems I: Regular Papers*, 60(3):733–742, 2012.
- [51] Donghyun Jeon, Seonghyun Kim, Beom Kwon, Hojae Lee, and Sanghoon Lee. Prototype filter design for qam-based filter bank multicarrier system. *Digital Signal Processing*, 57:66–78, 2016.
- [52] Imad A Shaheen and Abdelhalim Zekry. Design and implementation of fbmc/oqam transceiver for 5g wireless communication system. In *2019 International Conference on Promising Electronic Technologies (ICPET)*, pages 73–79. IEEE, 2019.
- [53] R Keerthana and S Rajaram. Fpga implementation of fbmc baseband modulator for 5g wireless communication. In *2019 2nd International Conference on Intelligent Computing, Instrumentation and Control Technologies (ICICT)*, volume 1, pages 718–723. IEEE, 2019.
- [54] Peter Lynch. The dolph–chebyshev window: A simple optimal filter. *Monthly weather review*, 125(4):655–660, 1997.
- [55] Robin Gerzaguet, Nikolaos Bartzoudis, Leonardo Gomes Baltar, Vincent Berg, Jean-Baptiste

- Doré, Dimitri Kténas, Oriol Font-Bach, Xavier Mestre, Miquel Payaró, Michael Färber, et al. The 5g candidate waveform race: a comparison of complexity and performance. *EURASIP Journal on Wireless Communications and Networking*, 2017(1):13, 2017.
- [56] Vikas Kumar, Mithun Mukherjee, and Jaime Lloret. Reconfigurable architecture of ufmf transmitter for 5g and its fpga prototype. *IEEE Systems Journal*, 14(1):28–38, 2019.
- [57] Nicola Michailow, Ivan Gaspar, Stefan Krone, Michael Lentmaier, and Gerhard Fettweis. Generalized frequency division multiplexing: Analysis of an alternative multi-carrier technique for next generation cellular systems. In *2012 International Symposium on Wireless Communication Systems (ISWCS)*, pages 171–175. IEEE, 2012.
- [58] Behrouz Farhang-Boroujeny and Hussein Moradi. Ofdm inspired waveforms for 5g. *IEEE Communications Surveys & Tutorials*, 18(4):2474–2492, 2016.
- [59] Arman Farhang, Nicola Marchetti, and Linda E Doyle. Low complexity gfdm receiver design: A new approach. In *2015 IEEE International Conference on Communications (ICC)*, pages 4775–4780. IEEE, 2015.
- [60] Jialing Li, Kenneth Kearney, Erdem Bala, and Rui Yang. A resource block based filtered ofdm scheme and performance comparison. In *ICT 2013*, pages 1–5. IEEE, 2013.
- [61] Xi Zhang, Ming Jia, Lei Chen, Jianglei Ma, and Jing Qiu. Filtered-ofdm-enabler for flexible waveform in the 5th generation cellular networks. In *2015 IEEE Global Communications Conference (GLOBECOM)*, pages 1–6. IEEE, 2015.
- [62] Stefania Sesia, Issam Toufik, and Matthew Baker. *LTE—the UMTS long term evolution: from theory to practice*. John Wiley & Sons, 2011.
- [63] Ricardo Tadashi Kobayashi and Taufik Abrão. Fbmc prototype filter design via convex optimization. *IEEE Transactions on Vehicular Technology*, 68(1):393–404, 2018.
- [64] Ivo Bizon Franco de Almeida and Luciano Leonel Mendes. Linear gfdm: A low out-of-band emission configuration for 5g air interface. In *2018 IEEE 5G World Forum (5GWF)*, pages 311–316. IEEE, 2018.
- [65] Myungsup Kim, Jiwon Jung, Ki-Man Kim, Wan-Jin Kim, et al. Spectral encapsulation to block the out-of-band emission of ofdm signals for future communications. In *2020 IEEE 91st Vehicular Technology Conference (VTC2020-Spring)*, pages 1–5. IEEE, 2020.
- [66] Daiming Qu, Fang Wang, Yan Wang, Tao Jiang, and Behrouz Farhang-Boroujeny. Improving spectral efficiency of fbmc-oqam through virtual symbols. *IEEE Transactions on Wireless Communications*, 16(7):4204–4215, 2017.
- [67] S Mohanraj and P Dananjayan. Performance analysis of gfdm system using ldgt for varying window. In *2019 IEEE International Conference on System, Computation, Automation and Networking (ICSCAN)*, pages 1–4. IEEE, 2019.
- [68] Hanna Bogucka and Andrea Conti. Degrees of freedom for energy savings in practical adaptive wireless systems. *IEEE Communications Magazine*, 49(6):38–45, 2011.
- [69] Kusha R Panta and Jean Armstrong. Effects of clipping on the error performance of ofdm in frequency selective fading channels. *IEEE Transactions on wireless communications*, 3(2):668–671, 2004.
- [70] D-Kyu Kim, D Shi, Y Park, and B Song. New peak-windowing for papr reduction of ofdm systems. In *Proc. Asia-Pacific Conference on Wearable Computing Systems (APWCS)*, pages 169–173, 2005.
- [71] Sulaiman A Aburakhia, Ehab F Badran, and Darwish AE Mohamed. Linear companding transform for the reduction of peak-to-average power ratio of ofdm signals. *IEEE Transactions on Broadcasting*, 55(1):155–160, 2009.
- [72] Thanatat Wattanasuwakull and Watit Benjapolakul. Papr reduction for ofdm transmission by using a method of tone reservation and tone injection. In *2005 5th International Conference on Information Communications & Signal Processing*, pages 273–277. IEEE, 2005.
- [73] Stefan H Muller and Johannes B Huber. Ofdm with reduced peak-to-average power ratio by optimum combination of partial transmit sequences. *Electronics letters*, 33(5):368–369, 1997.
- [74] Leonardo G Baltar, Frank Schaich, Markku Renfors, and Josef A Nossek. Computational complexity analysis of advanced physical layers based on multicarrier modulation. In *2011 Future Network & Mobile Summit*, pages 1–8. IEEE, 2011.
- [75] Thorsten Wild and Frank Schaich. A reduced complexity transmitter for uf-ofdm. In *2015 IEEE 81st Vehicular Technology Conference (VTC Spring)*, pages 1–6. IEEE, 2015.
- [76] Ivan Gaspar, Nicola Michailow, Ainoa Navarro, Eckhard Ohlmer, Stefan Krone, and Gerhard Fettweis. Low complexity gfdm receiver based on sparse frequency domain processing. In *2013 IEEE 77th Vehicular Technology Conference (VTC Spring)*, pages 1–6. IEEE, 2013.
- [77] Yahia Medjahdi, Sylvain Traverso, Robin Gerzaguet, Hmaied Shaiek, Rafik Zayani, David Demmer, Rostom Zakaria, Jean-Baptiste Doré, Mouna Ben Mabrouk, Didier Le Ruyet, et al. On the road to 5g: Comparative study of physical layer in mtc context. *IEEE Access*, 5:26556–26581, 2017.
- [78] Hyejin Kim, Yosub Park, Jintae Kim, and Daesik Hong. A low-complex svd-based f-ofdm. *IEEE Transactions on Wireless Communications*, 19(2):1373–1385, 2019.
- [79] François Horlin and André Bourdoux. *Digital compensation for analog front-ends: a new approach to wireless transceiver design*. John Wiley & Sons, 2008.
- [80] Khaled M Gharaibeh. *Nonlinear distortion in wireless systems: Modeling and simulation with MATLAB*. John Wiley & Sons, 2011.
- [81] Ahmed Hammoodi, Lukman Audah, and Montadar Abas Taher. Green coexistence for 5g waveform

- candidates: a review. *IEEE Access*, 7:10103–10126, 2019.
- [82] Junhui Zhao, Siying Lv, Lihua Yang, and Shanjin Ni. Genetic algorithm based prototype filter design for oriented side lobe energy suppression in fbmc system. *IEEE Access*, 8:8251–8261, 2020.
- [83] TobiasHidalgo Stitz, Tero Ihalainen, Ari Viholainen, and Markku Renfors. Pilot-based synchronization and equalization in filter bank multicarrier communications. *EURASIP Journal on Advances in Signal Processing*, 2010(1):741429, 2010.
- [84] Leonardo G Baltar, Amine Mezghani, and Josef A Nossek. Mlse and mmse subchannel equalization for filter bank based multicarrier systems: Coded and uncoded results. In *2010 18th European Signal Processing Conference*, pages 2186–2190. IEEE, 2010.
- [85] Alphan Sahin, Sultan Aldirmaz, Ismail Guvenc, and Huseyin Arslan. An investigation on number of effective taps for multicarrier schemes. In *2013 IEEE 77th Vehicular Technology Conference (VTC Spring)*, pages 1–5. IEEE, 2013.
- [86] David Falconer, S Lek Ariyavisitakul, Anader Benyamin-Seeyar, and Brian Eidson. Frequency domain equalization for single-carrier broadband wireless systems. *IEEE Communications Magazine*, 40(4):58–66, 2002.
- [87] Tero Ihalainen, Ari Viholainen, Tobias Hidalgo Stitz, Markku Renfors, and Maurice Bellanger. Filter bank based multi-mode multiple access scheme for wireless uplink. In *2009 17th European Signal Processing Conference*, pages 1354–1358. IEEE, 2009.
- [88] Dirk S Waldhauser, Leonardo G Baltar, and Josef A Nossek. Comparison of filter bank based multicarrier systems with ofdm. In *APCCAS 2006-2006 IEEE Asia Pacific Conference on Circuits and Systems*, pages 976–979. IEEE, 2006.
- [89] Tero Ihalainen, Tobias Hidalgo Stitz, Mika Rinne, and Markku Renfors. Channel equalization in filter bank based multicarrier modulation for wireless communications. *EURASIP Journal on Advances in Signal Processing*, 2007:1–18, 2006.
- [90] Tilde Fusco, Angelo Petrella, and Mario Tanda. Sensitivity of multi-user filter-bank multicarrier systems to synchronization errors. In *2008 3rd International Symposium on Communications, Control and Signal Processing*, pages 393–398. IEEE, 2008.
- [91] Jinfeng Du and Svante Signell. Pulse shape adaptivity in ofdm/oqam systems. In *Proceedings of the 2008 International Conference on Advanced Infocomm Technology*, pages 1–5, 2008.
- [92] Vidar Ringset, Helge Rustad, Frank Schaich, Jurgen Vandermot, and Montse Najar. Performance of a filterbank multicarrier (fbmc) physical layer in the wimax context. In *2010 Future Network & Mobile Summit*, pages 1–8. IEEE, 2010.
- [93] Qiwei Zhang, Andre BJ Kokkeler, and Gerard JM Smit. An oversampled filter bank multicarrier system for cognitive radio. In *2008 IEEE 19th International Symposium on Personal, Indoor and Mobile Radio Communications*, pages 1–5. IEEE, 2008.
- [94] Leonardo G Baltar, Dirk S Waldhauser, and Josef A Nossek. Out-of-band radiation in multicarrier systems: a comparison. In *Multi-Carrier Spread Spectrum 2007*, pages 107–116. Springer, 2007.
- [95] Dirk S Waldhauser, Leonardo G Baltar, and Josef A Nossek. Adaptive decision feedback equalization for filter bank based multicarrier systems. In *2009 IEEE International Symposium on Circuits and Systems*, pages 2794–2797. IEEE, 2009.
- [96] Jinfeng Du and Svante Signell. Novel preamble-based channel estimation for ofdm/oqam systems. In *2009 IEEE International Conference on Communications*, pages 1–6. IEEE, 2009.
- [97] Chrislin Lele, Pierre Siohan, and Rodolphe Legouable. 2 db better than cp-ofdm with ofdm/oqam for preamble-based channel estimation. In *2008 IEEE International Conference on Communications*, pages 1302–1306. IEEE, 2008.
- [98] Zsolt Kollar and Peter Horvath. Physical layer considerations for cognitive radio: Synchronization point of view. In *2011 IEEE 73rd Vehicular Technology Conference (VTC Spring)*, pages 1–5. IEEE, 2011.
- [99] Giovanni Cherubini, Evangelos Eleftheriou, and Sedat Olcer. Filtered multitone modulation for very high-speed digital subscriber lines. *IEEE Journal on Selected Areas in Communications*, 20(5):1016–1028, 2002.
- [100] Tero Ihalainen, Aïssa Ikhlef, Jérôme Louveaux, and Markku Renfors. Channel equalization for multi-antenna fbmc/oqam receivers. *IEEE transactions on vehicular technology*, 60(5):2070–2085, 2011.
- [101] Tobias Hidalgo Stitz, Tero Ihalainen, and Markku Renfors. Practical issues in frequency domain synchronization for filter bank based multicarrier transmission. In *2008 3rd International Symposium on Communications, Control and Signal Processing*, pages 411–416. IEEE, 2008.
- [102] Hamid Saeedi-Sourck, Yan Wu, Jan WM Bergmans, Saeed Sadri, and Behrouz Farhang-Boroujeny. Sensitivity analysis of offset qam multicarrier systems to residual carrier frequency and timing offsets. *Signal Processing*, 91(7):1604–1612, 2011.
- [103] Tilde Fusco and Mario Tanda. Blind frequency-offset estimation for ofdm/oqam systems. *IEEE Transactions on Signal Processing*, 55(5):1828–1838, 2007.
- [104] Dirk S Waldhauser, Leonardo G Baltar, and Josef A Nossek. Mmse subcarrier equalization for filter bank based multicarrier systems. In *2008 IEEE 9th Workshop on Signal Processing Advances in Wireless Communications*, pages 525–529. IEEE, 2008.
- [105] Dirk S Waldhauser, Leonardo G Baltar, and Josef A Nossek. Adaptive equalization for filter bank based multicarrier systems. In *2008 IEEE International Symposium on Circuits and Systems*, pages 3098–3101. IEEE, 2008.
- [106] Jinfeng Du. *Pulse shape adaptation and channel estimation in generalised frequency division multiplexing*

- systems. PhD thesis, KTH, 2008.
- [107] Fang-Ming Han and Xian-Da Zhang. Hexagonal multicarrier modulation: A robust transmission scheme for time-frequency dispersive channels. *IEEE Transactions on Signal Processing*, 55(5):1955–1961, 2007.
- [108] Sultan Aldirmaz, Ahmet Serbes, and Lutfiye Durak-Ata. Spectrally efficient ofdma lattice structure via toroidal waveforms on the time-frequency plane. *EURASIP Journal on Advances in Signal Processing*, 2010:1–8, 2010.
- [109] Fredrik Rusek and John B Anderson. Multistream faster than nyquist signaling. *IEEE Transactions on Communications*, 57(5):1329–1340, 2009.
- [110] Chrislin L  l  , J-P Javaudin, Rodolphe Legouable, Alexandre Skrzypczak, and Pierre Siohan. Channel estimation methods for preamble-based ofdm/oqam modulations. *European Transactions on Telecommunications*, 19(7):741–750, 2008.
- [111] C Lele, P Siohan, R Legouable, and J-P Javaudin. Preamble-based channel estimation techniques for ofdm/oqam over the powerline. In *2007 IEEE International Symposium on Power Line Communications and Its Applications*, pages 59–64. IEEE, 2007.
- [112] J-P Javaudin, Dominique Lacroix, and Alexandre Rouxel. Pilot-aided channel estimation for ofdm/oqam. In *The 57th IEEE Semiannual Vehicular Technology Conference, 2003. VTC 2003-Spring.*, volume 3, pages 1581–1585. IEEE, 2003.
- [113] M Alard. Construction of a multicarrier signal. *Patent WO*, 96(35):278, 1996.
- [114] Aissa Ikhlef and J  r  me Louveaux. An enhanced mmse per subchannel equalizer for highly frequency selective channels for fbmc/oqam systems. In *2009 IEEE 10th Workshop on Signal Processing Advances in Wireless Communications*, pages 186–190. IEEE, 2009.
- [115] Maurice Bellanger. Filter banks and ofdm-oqam for high throughput wireless lan. In *2008 3rd International Symposium on Communications, Control and Signal Processing*, pages 758–761. IEEE, 2008.
- [116] Frank Schaich. Filterbank based multi carrier transmission (fbmc)—evolving ofdm: Fbmc in the context of wimax. In *2010 European Wireless Conference (EW)*, pages 1051–1058. IEEE, 2010.
- [117] Tilde Fusco, Angelo Petrella, and Mario Tanda. Joint symbol timing and cfo estimation for ofdm/oqam systems in multipath channels. *EURASIP Journal on Advances in Signal Processing*, 2010(1):897607, 2009.
- [118] Wei Jiang and Malte Schellmann. Suppressing the out-of-band power radiation in multi-carrier systems: A comparative study. In *2012 IEEE Global Communications Conference (GLOBECOM)*, pages 1477–1482. IEEE, 2012.
- [119] Ari Viholainen, Maurice Bellanger, and Mathieu Huchard. of deliverable prototype filter and structure optimization. *Criterion*, 1:C2, 2009.
- [120] Rostom Zakaria, Didier Le Ruyet, and Maurice Bellanger. Maximum likelihood detection in spatial multiplexing with fbmc. In *2010 European Wireless Conference (EW)*, pages 1038–1041. IEEE, 2010.
- [121] Eleftherios Kofidis, Dimitrios Katselis, Athanasios Rontogiannis, and Sergios Theodoridis. Preamble-based channel estimation in ofdm/oqam systems: A review. *Signal Processing*, 93(7):2038–2054, 2013.
- [122] Ove Edfors, Magnus Sandell, J-J Van de Beek, Sarah Kate Wilson, and Per Ola Borjesson. Ofdm channel estimation by singular value decomposition. *IEEE Transactions on communications*, 46(7):931–939, 1998.
- [123] Hlaing Minn and Vijay K Bhargava. An investigation into time-domain approach for ofdm channel estimation. *IEEE Transactions on broadcasting*, 46(4):240–248, 2000.
- [124] Jianglei Ma, Ming Jia, Peiying Zhu, and Wen Tong. Scattered pilot pattern and channel estimation method for mimo-ofdm systems, July 24 2007. US Patent 7,248,559.
- [125] Yinsheng Liu, Zhenhui Tan, Hongjie Hu, Leonard J Cimini, and Geoffrey Ye Li. Channel estimation for ofdm. *IEEE Communications Surveys & Tutorials*, 16(4):1891–1908, 2014.
- [126] Mutsam A Jarajreh, Elias Giacomidis, Ivan Aldaya, Son Thai Le, Athanasios Tsokanos, Zabih Ghassemloooy, and Nick J Doran. Artificial neural network nonlinear equalizer for coherent optical ofdm. *IEEE Photonics Technology Letters*, 27(4):387–390, 2014.
- [127] Haim Primo, Yosef Stein, and Wei An. Equalization for ofdm communication, December 4 2012. US Patent 8,325,790.
- [128] Erdal Panayirci, Habib Senol, and H Vincent Poor. Joint channel estimation, equalization, and data detection for ofdm systems in the presence of very high mobility. *IEEE Transactions on Signal Processing*, 58(8):4225–4238, 2010.
- [129] Tareq Y Al-Naffouri, Ala A Dahman, Muhammad S Sohail, Weiyu Xu, and Babak Hassibi. Low-complexity blind equalization for ofdm systems with general constellations. *IEEE Transactions on Signal Processing*, 60(12):6395–6407, 2012.
- [130] Byungjoon Park, Hyunsoo Cheon, Eunseok Ko, Changeon Kang, and Daesik Hong. A blind ofdm synchronization algorithm based on cyclic correlation. *IEEE Signal Processing Letters*, 11(2):83–85, 2004.
- [131] Xianbin Wang, Tjeng Thiang Tjhung, Yiyan Wu, and Bernard Caron. Ser performance evaluation and optimization of ofdm system with residual frequency and timing offsets from imperfect synchronization. *IEEE Transactions on Broadcasting*, 49(2):170–177, 2003.
- [132] Hlaing Minn, Vijay K Bhargava, and Khaled Ben Letaief. A robust timing and frequency synchronization for ofdm systems. *IEEE transactions on wireless communications*, 2(4):822–839, 2003.
- [133] Tao Jiang and Yiyan Wu. An overview: Peak-to-average power ratio reduction techniques for ofdm signals. *IEEE Transactions on broadcasting*, 54(2):257–268, 2008.
- [134] NV Irukulapati, VK Chakka, and Abhay Jain. Slm based papr reduction of ofdm signal using new phase

- sequence. *Electronics letters*, 45(24):1231–1232, 2009.
- [135] Zs Kollar, L Varga, and K Czimer. Clipping-based iterative papr-reduction techniques for fbmc. In *OFDM 2012; 17th International OFDM Workshop 2012 (In-OWo'12)*, pages 1–7. VDE, 2012.
- [136] Yasir Rahmatallah and Seshadri Mohan. Peak-to-average power ratio reduction in ofdm systems: A survey and taxonomy. *IEEE communications surveys & tutorials*, 15(4):1567–1592, 2013.
- [137] Tarkesh Pande, David J Love, and James V Krogmeier. Reduced feedback mimo-ofdm precoding and antenna selection. *IEEE Transactions on Signal Processing*, 55(5):2284–2293, 2007.
- [138] Apurva N Mody and Gordon L Stuber. Synchronization for mimo ofdm systems. In *GLOBECOM'01. IEEE Global Telecommunications Conference (Cat. No. 01CH37270)*, volume 1, pages 509–513. IEEE, 2001.
- [139] Hongwei Yang. A road to future broadband wireless access: Mimo-ofdm-based air interface. *IEEE communications Magazine*, 43(1):53–60, 2005.
- [140] Alireza Attar, Oliver Holland, Mohammad Reza Nakhai, and A Hamid Aghvami. Interference-limited resource allocation for cognitive radio in orthogonal frequency-division multiplexing networks. *IET communications*, 2(6):806–814, 2008.
- [141] Mehdi Ghamari Adian and Hassan Aghaeinia. Optimal resource allocation for opportunistic spectrum access in multiple-input multiple-output-orthogonal frequency division multiplexing based cooperative cognitive radio networks. *IET Signal Processing*, 7(7):549–557, 2013.
- [142] Wenbo Cai, Chen Chen, Lin Bai, Ye Jin, and Jinho Choi. Subcarrier and power allocation scheme for downlink ofdm-noma systems. *IET Signal Processing*, 11(1):51–58, 2016.
- [143] Wenjia Cui, Daiming Qu, Tao Jiang, and Behrouz Farhang-Boroujeny. Coded auxiliary pilots for channel estimation in fbmc-oqam systems. *IEEE Transactions on Vehicular Technology*, 65(5):2936–2946, 2015.
- [144] Martin Fuhrwerk, Sanam Moghaddamnia, and Jürgen Peissig. Scattered pilot-based channel estimation for channel adaptive fbmc-oqam systems. *IEEE Transactions on Wireless Communications*, 16(3):1687–1702, 2017.
- [145] Gaëtan Ndo, Hao Lin, and Pierre Siohan. Fbmc/oqam equalization: Exploiting the imaginary interference. In *2012 IEEE 23rd International Symposium on Personal, Indoor and Mobile Radio Communications-(PIMRC)*, pages 2359–2364. IEEE, 2012.
- [146] Yahia Medjahdi, Michel Terre, Didier Le Ruyet, Daniel Roviras, and Ali Dziri. Performance analysis in the downlink of asynchronous ofdm/fbmc based multicellular networks. *IEEE transactions on wireless communications*, 10(8):2630–2639, 2011.
- [147] Dongjun Na and Kwonhue Choi. Low papr fbmc. *IEEE Transactions on Wireless Communications*, 17(1):182–193, 2017.
- [148] Han Wang, Xianpeng Wang, Lingwei Xu, and Wencai Du. Hybrid papr reduction scheme for fbmc/oqam systems based on multi data block pts and tr methods. *IEEE Access*, 4:4761–4768, 2016.
- [149] Rostom Zakaria and Didier Le Ruyet. A novel filter-bank multicarrier scheme to mitigate the intrinsic interference: Application to mimo systems. *IEEE Transactions on Wireless Communications*, 11(3):1112–1123, 2012.
- [150] Yassine Bendimerad and Fethi Tarik Bendimerad. Low complexity mimo-rb-f-ofdm systems using antenna selection technique. *IET Communications*, 14(1):152–157, 2019.
- [151] Haijian Zhang, Didier Le Ruyet, Daniel Roviras, and Hong Sun. Noncooperative multicell resource allocation of fbmc-based cognitive radio systems. *IEEE transactions on vehicular technology*, 61(2):799–811, 2011.
- [152] Juwendo Denis, Mylene Pischella, and Didier Le Ruyet. Energy-efficiency-based resource allocation framework for cognitive radio networks with fbmc/ofdm. *IEEE Transactions on Vehicular Technology*, 66(6):4997–5013, 2016.
- [153] Xiaojie Wang, Thorsten Wild, Frank Schaich, and Stephan ten Brink. Pilot-aided channel estimation for universal filtered multi-carrier. In *2015 IEEE 82nd Vehicular Technology Conference (VTC2015-Fall)*, pages 1–5. IEEE, 2015.
- [154] Rong Wang, Jingye Cai, Xiang Yu, and Sirui Duan. Compressive channel estimation for universal filtered multi-carrier system in high-speed scenarios. *Iet Communications*, 11(15):2274–2281, 2017.
- [155] Lei Zhang, Ayesha Ijaz, Pei Xiao, Muhammad Ali Imran, and Rahim Tafazolli. Mu-ufmc system performance analysis and optimal filter length and zero padding length design. *arXiv preprint arXiv:1603.09169*, 2016.
- [156] P Naga Rani and Ch Santhi Rani. Ufmc: The 5g modulation technique. In *2016 IEEE International Conference on Computational Intelligence and Computing Research (ICIC)*, pages 1–3. IEEE, 2016.
- [157] Frank Schaich and Thorsten Wild. Relaxed synchronization support of universal filtered multi-carrier including autonomous timing advance. In *2014 11th International Symposium on Wireless Communications Systems (ISWCS)*, pages 203–208. IEEE, 2014.
- [158] Hyunwoo Cho, Yan Yan, Gee-Kung Chang, and Xiaoli Ma. Asynchronous multi-user uplink transmissions for 5g with ufmc waveform. In *2017 IEEE Wireless Communications and Networking Conference (WCNC)*, pages 1–5. IEEE, 2017.
- [159] Wang Rong, Jingye Cai, and Xiang Yu. Low-complexity pts papr reduction scheme for ufmc systems. *Cluster Computing*, 20(4):3427–3440, 2017.
- [160] Stefano Buzzi, Carmen D'Andrea, Dejian Li, and Shulan Feng. Mimo-ufmc transceiver schemes for millimeter-wave wireless communications. *IEEE Transactions on Communications*, 67(5):3323–3336, 2019.
- [161] Xiaoming Chen, Shuai Zhang, and Anxue Zhang. On mimo-ufmc in the presence of phase noise and antenna mutual coupling. *Radio Science*, 52(11):1386–1394, 2017.

- [162] Hyunsoo Kim, Jonghyun Bang, Sooyong Choi, and Daesik Hong. Resource block management for uplink ufmc systems. In *2016 IEEE Wireless Communications and Networking Conference*, pages 1–4. IEEE, 2016.
- [163] Paolo Del Fiorentino, Carmine Vitiello, Vincenzo Lottici, Erica Debels, Jeroen Van Hecke, Marc Moeneclaey, Filippo Giannetti, and Marco Luise. Resource allocation in short packets bic-ufmc transmission for internet of things. In *2016 IEEE globecom workshops (GC Wkshps)*, pages 1–6. IEEE, 2016.
- [164] Usa Vilaipornsawai and Ming Jia. Scattered-pilot channel estimation for gfdm. In *2014 IEEE Wireless Communications and Networking Conference (WCNC)*, pages 1053–1058. IEEE, 2014.
- [165] Zhenyu Na, Zheng Pan, Mudi Xiong, Xin Liu, Weidang Lu, Yongjian Wang, and Lisheng Fan. Turbo receiver channel estimation for gfdm-based cognitive radio networks. *IEEE Access*, 6:9926–9935, 2018.
- [166] Jinkyoo Jeong, Yosub Park, Sungwoo Weon, Jintae Kim, Sooyong Choi, and Daesik Hong. Eigendecomposition-based gfdm for interference-free data transmission and pilot insertion for channel estimation. *IEEE Transactions on Wireless Communications*, 17(10):6931–6943, 2018.
- [167] Jie Zhong, Gaojie Chen, Juquan Mao, Shuping Dang, and Pei Xiao. Iterative frequency domain equalization for mimo-gfdm systems. *IEEE Access*, 6:19386–19395, 2018.
- [168] Matt Carrick and Jeffrey H Reed. Improved gfdm equalization in severe frequency selective fading. In *2017 IEEE 38th Sarnoff Symposium*, pages 1–6. IEEE, 2017.
- [169] Shashank Tiwari and Suvra Sekhar Das. Low-complexity joint-mmse gfdm receiver. *IEEE Transactions on Communications*, 66(4):1661–1674, 2017.
- [170] Ivan S Gaspar, Luciano L Mendes, Nicola Michailow, and Gerhard Fettweis. A synchronization technique for generalized frequency division multiplexing. *EURASIP Journal on Advances in Signal Processing*, 2014(1):67, 2014.
- [171] Po-Sen Wang and David W Lin. Maximum-likelihood blind synchronization for gfdm systems. *IEEE Signal Processing Letters*, 23(6):790–794, 2016.
- [172] Zhenyu Na, Mengshu Zhang, Mudi Xiong, Junjuan Xia, Xin Liu, and Weidang Lu. Pseudo-noise sequence based synchronization for generalized frequency division multiplexing in 5g communication system. *IEEE Access*, 6:14812–14819, 2018.
- [173] Zahra Sharifian, Mohammad Javad Omid, Arman Farhang, and Hamid Saeedi-Sourck. Polynomial-based compressing and iterative expanding for papr reduction in gfdm. In *2015 23rd Iranian Conference on Electrical Engineering*, pages 518–523. IEEE, 2015.
- [174] Zahra Sharifian, Mohammad Javad Omid, Hamid Saeedi-Sourck, and Arman Farhang. Linear precoding for papr reduction of gfdma. *IEEE Wireless Communications Letters*, 5(5):520–523, 2016.
- [175] Shravan Kumar Bandari, Venkata Mani Vakamulla, and Anastasios Drosopoulos. Papr analysis of wavelet based multitaper gfdm system. *AEU-International Journal of Electronics and Communications*, 76:166–174, 2017.
- [176] Maximilian Matthé, Dan Zhang, and Gerhard Fettweis. Sphere-decoding aided sic for mimo-gfdm: Coded performance analysis. In *2016 International Symposium on Wireless Communication Systems (ISWCS)*, pages 165–169. IEEE, 2016.
- [177] Maximilian Matthé, Dan Zhang, and Gerhard Fettweis. Low-complexity iterative mmse-pic detection for mimo-gfdm. *IEEE Transactions on Communications*, 66(4):1467–1480, 2017.
- [178] Dan Zhang, Luciano Leonel Mendes, Maximilian Matthé, Ivan Simões Gaspar, Nicola Michailow, and Gerhard P Fettweis. Expectation propagation for near-optimum detection of mimo-gfdm signals. *IEEE Transactions on Wireless Communications*, 15(2):1045–1062, 2015.
- [179] Ali Mokdad, Paeiz Azmi, and Nader Mokari. Radio resource allocation for heterogeneous traffic in gfdm-noma heterogeneous cellular networks. *IET Communications*, 10(12):1444–1455, 2016.
- [180] Arturo González, Sebastian Kühlmorgen, Andreas Festag, and Gerhard Fettweis. Resource allocation for block-based multi-carrier systems considering qos requirements. In *GLOBECOM 2017-2017 IEEE Global Communications Conference*, pages 1–7. IEEE, 2017.
- [181] Lei Zhang, Ayesha Ijaz, Pei Xiao, Mehdi M Molu, and Rahim Tafazolli. Filtered ofdm systems, algorithms, and performance analysis for 5g and beyond. *IEEE Transactions on Communications*, 66(3):1205–1218, 2017.
- [182] Peter Zillmann, Wolfgang Rave, and Gerhard Fettweis. Turbo equalization for clipped and filtered cofdm signals. In *2007 IEEE International Conference on Communications*, pages 4335–4340. IEEE, 2007.
- [183] Mouna Ben Mabrouk, Marwa Chafii, Yves Louet, and Faouzi Bader. A precoding-based papr reduction technique for uf-ofdm and filtered-ofdm modulations in 5g systems. In *European Wireless 2017; 23th European Wireless Conference*, pages 1–6. VDE, 2017.
- [184] Jialing Li, Erdem Bala, and Rui Yang. Resource block filtered-ofdm for future spectrally agile and power efficient systems. *Physical Communication*, 11:36–55, 2014.
- [185] AKM Baki, Rafee Al Ahsan, and Azwad Awsaf. Novel methods of filtering for fbmc/ufmc based 5g communication systems. In *2019 7th International Conference on Smart Computing & Communications (ICSCC)*, pages 1–4. IEEE, 2019.